Fault-Tolerant Control of Fractional-Order Multi-Agent Systems Using Interval Type-2 Fuzzy Logic and Adaptive Observers

Qunge Hu[1,*] and Azmat Ullah Khan Niazi[2,*]

[1] College of Civil Engineering and Architecture, Zhejiang University of Water Resources and Electric Power, Hangzhou, 310018, China

[2] Department of Mathematics and Statistics, The University of Lahore, Sargodha, 40100, Pakistan

INFORMATION

Keywords:
Multi-agent systems
actuator faults
uncertainty handling
IT-II fuzzy set
fuzzy dynamic containment control
lyapunov-krasovskii functional

DOI: 10.23967/j.rimni.2026.10.76025

SCIPEDIA Revista Internacional de Métodos Numéricos para Cálculo y Diseño en Ingeniería

Revista Internacional Métodos numéricos para cálculo y diseño en ingeniería RIMNI in cooperation with CIMNE

Fault-Tolerant Control of Fractional-Order Multi-Agent Systems Using Interval Type-2 Fuzzy Logic and Adaptive Observers

Qunge Hu[1,*] **and Azmat Ullah Khan Niazi**[2,*]

[1]College of Civil Engineering and Architecture, Zhejiang University of Water Resources and Electric Power, Hangzhou, 310018, China

[2]Department of Mathematics and Statistics, The University of Lahore, Sargodha, 40100, Pakistan

ABSTRACT

This study addresses the containment control challenge in heterogeneous, nonlinear fractional-order multi-agent systems (MASs) operating under uncertainties, actuator faults, unknown nonlinearities, and mixed time-varying delays, with the aim of ensuring stability and robust performance in realistic environments. A fully distributed adaptive observer is developed for each follower to estimate leader state information using only local neighbor data, and an interval type-2 fuzzy logic system is integrated into the adaptive control law to approximate unknown dynamics and compensate for actuator faults. Stability is established via a newly formulated fractional-order Lyapunov Krasovskii functional combined with inequality analysis, and the method's effectiveness is verified through simulations on a fractional-order Lorenz-based MAS. Results show that the proposed approach achieves precise containment control despite actuator efficiency loss and bias faults, with an root-mean-square error (RMSE) of 0.028, a settling time of 1.2 s, and disturbance rejection within 0.8 s, outperforming classical Proportion, Integral, Differential (PID) and Type-1 fuzzy controllers. These findings demonstrate that the proposed framework not only enhances fault tolerance and tracking accuracy but is also computationally efficient, making it suitable for real-time applications such as UAV swarms, autonomous vehicles, and cooperative robotics.

OPEN ACCESS

Received: 12/11/2025

Accepted: 22/12/2025

Published: 29/05/2026

DOI
10.23967/j.rimni.2026.10.76025

Keywords:
Multi-agent systems
actuator faults
uncertainty handling
IT-II fuzzy set
fuzzy dynamic containment control
lyapunov-krasovskii functional

1 Introduction

Multi-agent systems (MASs) have become a paramount research topic due to their wide-ranging applications across engineering and technology, spanning from transportation and logistics to defense and space exploration. The core goal in many of these applications, such as autonomous vehicles and drone swarms, is to achieve complex collective behaviors, including consensus, formation control, and containment [1]. For instance, sophisticated control strategies are essential for handling complex scenarios like curvilinear multilane merging [2] or maintaining distributed formation of fixed-wing UAV swarms under performance constraints [3]. The ability of MASs to perform tasks that are beyond the capability of a single agent has motivated extensive research into their control, coordination, and reliability [4]. Addressing the inherent complexities of coupled dynamics and communication

*Correspondence: Qunge Hu, Azmat Ullah Khan Niazi (13666605205@163.com, azmatullah.khan@math.uol.edu.pk).

topologies remains a central challenge, requiring robust and intelligent control architectures for effective deployment [5].

The coordination of multiple agents often necessitates advanced planning and control mechanisms to guarantee precise and collision-free movement in dynamic environments. Path planning strategies must account for various factors, including the physical constraints of the agents and external environmental changes [6]. In dynamic settings, online optimization strategies, such as those used for planetary rover escape entrapment [7], and advanced techniques like Multi-Agent Reinforcement Learning (MARL) for network-wide traffic signal control [8], are crucial for real-time decision-making. Furthermore, achieving high-performance real-time dynamic obstacle avoidance for robotic manipulators requires complex parallel control techniques and cost-function modulation [9], while human-machine shared steering control demands efficient deep reinforcement learning with expert demonstrations [10]. Such precision is vital for autonomous vehicles, where event-triggered collaborative control is needed for systems like four-wheel independent steering [11]. Classical control theory predominantly relies on integer-order models. However, fractional-order (FO) calculus provides a powerful framework for modeling systems with inherent memory effects and non-local properties, offering increased accuracy for describing complex physical processes. Incorporating FO dynamics into MAS models allows for a more realistic representation of various real-world phenomena. To ensure timely and high-quality transient performance, control methods have increasingly focused on guaranteeing convergence within a fixed or predefined time. This has led to the development of techniques like predefined-time stabilization for high-order systems [12] and fixed-time equivalent-input-disturbance approaches for robust disturbance rejection [13]. Such time-based controls are also critical in fields like aerospace, exemplified by the quantized predefined-time control for heavy-lift launch vehicles [14] and event-triggered predefined-time anti-unwinding attitude tracking for spacecraft [15].

Real-world operational environments invariably expose MASs to unmodeled dynamics, unknown nonlinearities, and external disturbances. The presence of time-varying delays, both in communication and system dynamics, further complicates control design, as demonstrated by studies on the consensus of second-order multi-agent systems with intentional delays [16]. Ensuring robust performance requires control strategies that can effectively compensate for these imperfections. This includes PDE-based observation for systems with distributed infinite input and output delays [17] and transient frequency-voltage support strategies based on perturbation observers and funnel control for power systems [18]. Furthermore, in complex interconnected systems, such as those subject to faults, decentralized optimal control methods based on dynamic high-gain techniques are necessary to maintain stability and performance [19], alongside robust control techniques that utilize tools like Nash Equilibrium Theory for complex manipulation tasks [20].

Given the critical nature of many MAS applications, such as autonomous transportation and power systems, system reliability is paramount. A single component failure can lead to catastrophic mission failure or safety hazards. Therefore, Fault-Tolerant Control (FTC) systems are essential for maintaining stability and acceptable performance even when component faults (e.g., actuator bias or partial effectiveness loss) occur [21]. Research in this area focuses on both active and passive FTC strategies. Active FTC, which relies on fault detection and isolation (FDI) mechanisms, is crucial for systems like fault-tolerant multiparallel converters and for detecting abnormal states of aero-engines during maneuvering flight [22]. Furthermore, safety-critical systems, including the Intelligent Event Triggered Lane Keeping Security Control for Autonomous Vehicles under Denial-of-Service (DoS) attacks, underscore the need for resilient control architectures [23]. In a broader context, the

overall reliability of a system, measured by importance based on performance loss, is a foundational consideration in system design [24] and is tied closely to the life cycle of the system [25].

Before a system can implement FTC, the fault must be accurately detected and identified. Fault diagnosis and prognosis are specialized fields dedicated to this task, with growing relevance across various engineering domains. Modern techniques leverage advanced signal processing and data-driven methods for high-speed analysis, such as the ParallelGraphNet-driven multi-sensor optimization for elevator fault diagnosis [26] and weak time-varying fault indicator detection for complex gearboxes [27]. Industrial equipment, such as Permanent Magnet Synchronous Motors (PMSMs), requires robust diagnosis of faults like partial demagnetization under complex working conditions [28]. Furthermore, condition monitoring is being advanced through techniques like mechanism-guided intelligent enhancement for early aging information in winding insulation [29], digital twin modeling for elevators [30], degradation twin modeling for rolling bearings [31], and even novel hardware like hybrid triboelectric generators for wireless monitoring of aero-engine bearings [32].

In distributed MASs, agents often lack direct access to the full state information of the leader or all neighbors, relying only on local measurements. This necessitates the design of robust, distributed state observers to estimate unknown states. The adaptive nature of these observers allows them to track the leader's dynamics or estimate unknown parameters and fault magnitude in real time. For instance, the use of neurodynamics-based visual servo predictive control improves the smooth movement of logistics omnidirectional robots [33]. Control input is often optimized by mechanisms like event-triggered control to conserve communication bandwidth, a strategy employed in systems like neural learning tracking control for pneumatic muscle joints [34] and for securing autonomous vehicles. The combination of adaptive estimation, as seen in RBFNN-based parameter adaptive sliding mode control for uncertain TQUAVs [35] and recurrent neural network-based sliding mode control for uncertain tilting quadrotors [36], and robust control is key to dealing with state-space limitations.

To cope with system nonlinearities that cannot be precisely modeled, researchers have increasingly turned to intelligent control techniques, particularly fuzzy logic and neural networks. These approximators can reconstruct complex functions and compensate for unknown dynamics within the control law [37]. Interval Type-2 Fuzzy Logic Systems (IT2FLS), in particular, offer enhanced robustness over their Type-1 counterparts by modeling linguistic and numerical uncertainties in membership functions, making them superior for handling highly uncertain environments. Furthermore, integrating machine learning, such as dynamic graph meta-learning for cross-category fault diagnosis [38], and sensor fusion technologies for intelligent auxiliary systems in power wheelchairs [39], has broadened the scope of intelligent control, allowing systems to learn from experience and adapt to new scenarios.

Gradient-based time-delay optimization methods for fractional optimal control problems with Caputo–Fabrizio derivatives have been developed to efficiently handle discretized fractional systems using Adams–Bashforth and trapezoidal schemes [40], and have been successfully applied to fractional-order infectious disease models to optimize intervention strategies under realistic cost structures [41]. These developments establish a solid methodological foundation for further research on time-delay optimization in fractional-order dynamical systems. However, most existing studies focus primarily on optimization and modeling accuracy, while paying limited attention to robustness and fault tolerance in complex dynamical environments. Moreover, existing solutions often neglect either the fractional-order characteristics or the robustness enhancement offered by higher-order fuzzy logic systems. Motivated by this gap, our motivation is to bridge it by proposing a unified framework. This framework must combine a distributed adaptive observer for leader state estimation with an Interval Type-2 Fuzzy Logic System to robustly approximate all unknown terms and actively

compensate for actuator faults, ensuring reliability in dynamic and safety-critical applications like multi-asteroid exploration missions [42], and energy regenerative suspension systems [43]. This level of integrated fault tolerance is crucial for modern engineering systems, including novel actuators that require sophisticated control [44].

From a control-theoretic perspective, adaptive and intelligent control strategies have been extensively studied for nonlinear and chaotic systems, particularly when uncertainties and fractional-order dynamics are present. Financial and economic systems modeled as fractional-order chaotic systems have served as important benchmarks for developing robust control methodologies, due to their strong nonlinearities, uncertainties, and sensitivity to disturbances. Adaptive neural–fuzzy control schemes have been shown to effectively approximate unknown nonlinear dynamics and guarantee stability for hyperchaotic systems with complex nonlinear structures [45]. In addition, adaptive finite-time sliding mode control has been successfully applied to fractional-order chaotic systems, providing fast convergence and strong robustness against uncertainties and disturbances [46]. These studies provide valuable theoretical foundations and practical insights for the development of adaptive, fault-tolerant, and fuzzy-based control strategies for complex fractional-order multi-agent systems.

In this paper, we propose a novel Interval Type-2 Fuzzy Logic System-based Fault-Tolerant Containment Control approach for heterogeneous, nonlinear Fractional-Order Multi-Agent Systems subject to actuator faults, unknown nonlinearities, and mixed time-varying delays. The primary contributions of this work are threefold: First, we develop a fully distributed adaptive observer to estimate the leader's state using only local neighbor information, which is a necessity in real-world distributed control systems [6]. Second, we integrate the IT2FLS into the adaptive control law to achieve robust approximation of system uncertainties and provide dynamic compensation for actuator faults, thereby guaranteeing control stability and tracking performance. Third, we establish the stability of the entire closed-loop system using a newly formulated fractional-order Lyapunov-Krasovskii functional, demonstrating guaranteed convergence of the containment error.

The remainder of this paper is organized as follows: Section 2 presents preliminaries and relevant lemmas; Section 3 describes the problem formulation and proposed design; Section 4 provides stability analysis and theoretical results; Section 5 reports simulation results and comparisons; Section 6 concludes the paper and discusses future work [4,9,11].

2 Preliminaries

This research focuses on a MAS made up of Q follower agents and R leader agents. The interaction between the MASs can be represented using a directed communication topology $G = \{V, E\}$, where $V = \{v_1, \ldots, v_N\}$ denotes the set of nodes, and $E \subseteq V \times V$ indicates the set of edges. Additionally, the distance from a point $y \in \mathbb{N}^n$ to a set $D \subseteq \mathbb{N}^n$, denoted as $\mathrm{dist}(y, D)$, is measured using the Euclidean norm and is defined as

$$\mathrm{dist}(y, D) = \inf_{z \in D} \|y - z\|_2.$$

2.1 Definitions and Lemmas

Definition 1: *[47]. The Riemann-Liouville fractional integral of order α, for an integrable function $g(t) : [0, \infty) \to \mathbb{R}$ defined as*

$$I^{\alpha} g(t) = \frac{1}{\Gamma(\alpha)} \int_0^t \frac{g(\tau)}{(t-\tau)^{1-\alpha}} \, d\tau, \quad 0 < \alpha < 1,$$

where $\Gamma(\alpha)$ *is the Gamma function given by* $\Gamma(\alpha) = \int_0^\infty e^{-t}t^{\alpha-1}\,dt$.

Definition 2: *[47]. The Caputo derivative of fractional order* α *of a function* $g \in C^1([t_0, +\infty), \mathbb{R})$ *is defined by*

$$t_0 D_t^\alpha g(t) = \frac{1}{\Gamma(1-\alpha)} \int_{t_0}^{t} \frac{g'(\tau)}{(t-\tau)^\alpha}\, d\tau,$$

where $0 < \alpha < 1$, $0 \le t_0 \le t$. *When* $t_0 = 0$, $t_0 D_t^\alpha f(t)$ *becomes* $D_t^\alpha f(t)$.

Lemma 1: *[47]. Let* $x(t) \in \mathbb{R}^n$ *be a differentiable time-dependent function. Then, for any time instant* $t \ge 0$, *we have*

$$D^\alpha x^T(t)\mathcal{P}x(t) \le 2x^T(t)\mathcal{P}(D^\alpha x(t)),$$

where $\mathcal{P} \in \mathbb{R}^{n\times n}$ *is a symmetric positive definite matrix. The fractional order* α *satisfies the condition* $0 < \alpha < 1$.

Lemma 2: *[48]. Let* $\zeta : [\xi - \nu(\xi), \xi] \to \mathbb{R}^n$ *be a vector function. Then, the following inequality holds:*

$$-\int_{\xi-\nu(\xi)}^{\xi} \zeta^T(\sigma)P\zeta(\sigma)d\sigma \le -\frac{1}{\nu(\xi)}\left(\int_{\xi-\nu(\xi)}^{\xi}\zeta(\sigma)d\sigma\right)^T P\left(\int_{\xi-\nu(\xi)}^{\xi}\zeta(\sigma)d\sigma\right),$$

where $\nu(\xi) > 0$ *and* $P > 0$ *is a matrix.*

Lemma 3: *[35,40]. If* $x(t) \in C^1([t_0, +\infty), \mathbb{R})$ *and* $0 < \beta < 1$, *then*

$$I^\beta(D^\beta x(t)) = x(t) - x(0).$$

Lemma 4: *Let* $g(s)$ *is a continuous function, then*

$$I^{\gamma_1}(I^{\gamma_2}g(s)) = I^{\gamma_2}(I^{\gamma_1}g(s)) = I^{\gamma_1+\gamma_2}(g(s)),$$

where $0 < \gamma_p \le 1$, $p = 1, 2$.

Lemma 5 (Barbalat Lemma): *Let* $\varphi : \mathbb{R} \to \mathbb{R}$ *be a uniformly continuous function on the interval* $[0, \infty)$. *If*

$$\lim_{t\to\infty} \int_0^t \varphi(s)\, ds$$

exists and is bounded, then

$$\lim_{t\to\infty} \varphi(t) = 0.$$

2.2 Introduction to Interval Type-II Fuzzy Logic Systems

This section offers a brief introduction to the descriptive method for IT-II FLSs as discussed in [22]. The $k_1k_2\ldots k_n$-th rule in an IT-II FLS can be structured as given by:

$$\mathcal{R}^{i_1 i_2 \ldots i_n} : \text{IF } \varsigma_1 \text{ is } \tilde{\mathcal{F}}_1^{i_1}, \ldots, \varsigma_n \text{ is } \tilde{\mathcal{F}}_n^{i_n}, \text{ THEN } z \text{ is } \left[\underline{\theta}_{i_1 i_2 \ldots i_n}, \overline{\theta}_{i_1 i_2 \ldots i_n}\right]$$

where $i_j = 1, 2, \ldots, r_j, j = 1, 2, \ldots, n$. In the IT-II FLS, $\varsigma = [\varsigma_1, \varsigma_2, \ldots, \varsigma_n]^T$ is the input variable, and z is the output variable. An IT-II fuzzy set $\tilde{\mathcal{F}}_j^{i_j}$ belongs to the antecedent part, and output interval of the system is given by $\left[\underline{\theta}_{i_1 i_2 \ldots i_n}, \overline{\theta}_{i_1 i_2 \ldots i_n}\right]$.

This article employs the model reduction approach to determine the system's final output:

$$z = \varsigma \frac{\sum_{i_1=1}^{r_1} \cdots \sum_{i_n=1}^{r_n} \underline{\theta}_{i_1 i_2 \ldots i_n} \prod_{j=1}^{n} \underline{\mu}_{\mathcal{F}_j^{i_j}}(\varsigma_j)}{\sum_{i_1=1}^{r_1} \cdots \sum_{i_n=1}^{r_n} \prod_{j=1}^{n} \underline{\mu}_{\mathcal{F}_j^{i_j}}(\varsigma_j)} + (1-\varsigma) \frac{\sum_{i_1=1}^{r_1} \cdots \sum_{i_n=1}^{r_n} \overline{\theta}_{i_1 i_2 \ldots i_n} \prod_{j=1}^{n} \overline{\mu}_{\mathcal{F}_j^{i_j}}(\varsigma_j)}{\sum_{i_1=1}^{r_1} \cdots \sum_{i_n=1}^{r_n} \prod_{j=1}^{n} \overline{\mu}_{\mathcal{F}_j^{i_j}}(\varsigma_j)} \tag{1}$$

where $\underline{\mu}_{\mathcal{F}_j^{i_j}}(\varsigma_j)$ and $\overline{\mu}_{\mathcal{F}_j^{i_j}}(\varsigma_j)$ denote the lower and upper membership functions, respectively. The $0 \leq \varsigma \leq 1$ represents the regulating factor.

To solve the fuzzy system (1) we define the following parameters and fuzzy basis functions:

$$\underline{\vartheta}_{i_1 i_2 \ldots i_n} = \varsigma \underline{\theta}_{i_1 i_2 \ldots i_n}, \quad \overline{\vartheta}_{i_1 i_2 \ldots i_n} = (1-\varsigma)\overline{\theta}_{i_1 i_2 \ldots i_n},$$

$$\mathcal{L}_{i_1 i_2 \ldots i_n}(\varsigma) = \frac{\sum_{i_1=1}^{r_1} \sum_{i_2=1}^{r_2} \cdots \sum_{i_n=1}^{r_n} \prod_{j=1}^{n} \underline{\mu}_{\mathcal{F}_j}^{i_j}(\varsigma_j)}{\sum_{i_1=1}^{r_1} \sum_{i_2=1}^{r_2} \cdots \sum_{i_n=1}^{r_n} \prod_{j=1}^{n} \underline{\mu}_{\mathcal{F}_j}^{i_j}(\varsigma_j)},$$

$$\mathcal{R}_{i_1 i_2 \ldots i_n}(\varsigma) = \frac{\sum_{i_1=1}^{r_1} \sum_{i_2=1}^{r_2} \cdots \sum_{i_n=1}^{r_n} \prod_{j=1}^{n} \overline{\mu}_{\mathcal{F}_j}^{i_j}(\varsigma_j)}{\sum_{i_1=1}^{r_1} \sum_{i_2=1}^{r_2} \cdots \sum_{i_n=1}^{r_n} \prod_{j=1}^{n} \overline{\mu}_{\mathcal{F}_j}^{i_j}(\varsigma_j)}, \tag{2}$$

where $\mathcal{L}_{i_1 i_2 \ldots i_n}(\varsigma)$ is left fuzzy base and $\mathcal{R}_{i_1 i_2 \ldots i_n}(\varsigma)$ is the right fuzzy base function. The output z is the weighted sum of these fundamental basis functions, represented as:

$$z = \sum_{i_1=1}^{r_1} \sum_{i_2=1}^{r_2} \cdots \sum_{i_n=1}^{r_n} \left(\underline{\vartheta}_{i_1 i_2 \ldots i_n} \mathcal{L}_{i_1 i_2 \ldots i_n}(\varsigma) + \overline{\vartheta}_{i_1 i_2 \ldots i_n} \mathcal{R}_{i_1 i_2 \ldots i_n}(\varsigma) \right). \tag{3}$$

We can rewrite Eq. (3) in a more compact vector form as follows:

$$z = \Theta_l^T \mathcal{L}_l(\varsigma) + \Theta_r^T \mathcal{R}_r(\varsigma),$$

where Θ_l^T and Θ_r^T are the coefficients associated with the basis functions.

Table 1 shows a representative subset of the fuzzy inference rules employed in the IT-II FLS. Each rule $\mathcal{R}_{i_1 i_2}$ is defined based on a combination of the input variables $(\varsigma_1, \varsigma_2)$, typically representing the tracking error and its derivative, and the corresponding fuzzy sets $(\tilde{\mathcal{F}}_1^{i_1}, \tilde{\mathcal{F}}_2^{i_2})$. The output of each rule is an interval $\left[\underline{\vartheta}_{i_1 i_2}, \overline{\vartheta}_{i_1 i_2}\right]$, capturing the uncertainty and flexibility in the control response. These intervals are selected heuristically based on the expected control action under each input condition stronger actions for large deviations and narrower intervals near equilibrium. This rule structure enables the IT-II FLS to provide robust, adaptive control in the presence of nonlinearities and modeling uncertainties.

Table 1: Fuzzification and defuzzification rules for the IT-II FLS

Rule #	Input pair $(\varsigma_1, \varsigma_2)$	Antecedent sets $(\tilde{\mathcal{F}}_1^{i_1}, \tilde{\mathcal{F}}_2^{i_2})$	Output interval $\left[\underline{\vartheta}_{i_1 i_2}, \overline{\vartheta}_{i_1 i_2}\right]$	Support range
$\mathcal{R}_{11}$	(NL, NS)	$(\tilde{\mathcal{F}}_1^1, \tilde{\mathcal{F}}_2^1)$	$[-0.8, -0.5]$	$[-1.0, -0.3]$

(Continued)

Table 1 (continued)

Rule #	Input pair $(\varsigma_1, \varsigma_2)$	Antecedent sets $(\tilde{\mathcal{F}}_1^{i_1}, \tilde{\mathcal{F}}_2^{i_2})$	Output interval $\left[\underline{\vartheta}_{i_1 i_2}, \overline{\vartheta}_{i_1 i_2}\right]$	Support range
$\mathcal{R}_{22}$	(NS, Z)	$(\tilde{\mathcal{F}}_1^2, \tilde{\mathcal{F}}_2^2)$	$[-0.4, -0.2]$	$[-0.6, 0.0]$
$\mathcal{R}_{33}$	(Z, Z)	$(\tilde{\mathcal{F}}_1^3, \tilde{\mathcal{F}}_2^3)$	$[-0.1, 0.1]$	$[-0.3, 0.3]$
$\mathcal{R}_{44}$	(PS, PS)	$(\tilde{\mathcal{F}}_1^4, \tilde{\mathcal{F}}_2^4)$	$[0.2, 0.4]$	$[0.0, 0.6]$
$\mathcal{R}_{55}$	(PL, PL)	$(\tilde{\mathcal{F}}_1^5, \tilde{\mathcal{F}}_2^5)$	$[0.5, 0.8]$	$[0.3, 1.0]$

3 Problem Formulation

This article examines a complex nonlinear fractional-order multi-agent system (FO MAS) that incorporates uncertainties, node faults, and mixed time-varying delays.

$$\begin{aligned}
&\mathcal{D}^{\alpha}\mathbf{s}_{it} = A_i\mathbf{s}_{it} + g_i(\mathbf{s}_{it}, d_{it}, \tau_{it}) + \beta_i^F u_i(t) + \eta_i^F u_{si}(t) + \Delta_{it}, \quad i \in \mathcal{F}_s = \{1, 2, \ldots, Q\},\\
&\mathcal{D}^{\alpha}\nu_{kt} = \Phi_k(\nu_{kt}), \quad k \in \mathcal{L}_s = \{Q+1, \ldots, Q+R\}.
\end{aligned} \tag{4}$$

where Q and R represent the number of followers and leaders, respectively. $\mathbf{s}_{it}$ denotes the state of i-th follower, the unknown constant β_i^F satisfies $0 < \beta^F < \beta_i^F < \overline{\beta}^F \leq 1$, which indicates the actuator efficiency loss fault. $\eta_i^F \in \{0, 1\}$, $u_{si}(t)$ is the bias-actuator fault, which satisfies $|u_{si}(t)| \leq \overline{u}_{si}$ and $\overline{u}_{si} \in \mathbb{R}_{\geq 0}$ while ν_{kt} is the k-th leader. Matrix A_i is a constant matrix which is unknown and it belongs to $\mathbb{R}^{n\times n}$. The uncertain parameter Δ_{it} is uncertain parameter that satisfies $\|\Delta_{it}\| \leq \Delta_i$, where Δ_i is a novel constant. The function $\Phi_k(\nu_{kt})$ is a novel function that is bounded.

Function $g_i(\mathbf{s}_{it}, d_{it}, \tau_{it})$ is expressed in the following form:

$$g_i(\mathbf{s}_{it}, d_{it}, \tau_{it}) = g_{i1}(\mathbf{s}_{i(t-d_{it})}) + \int_{t-\tau_{it}}^{t} g_{i2}(\mathbf{s}_{is})\, ds + g_{i3}(\mathbf{s}_{it}), \tag{5}$$

where the variables d_{it} and τ_{it} denote time-dependent delays and satisfy the given conditions $0 < \dot{d}_{it} \leq \overline{d}_i < 1$, $0 < \dot{\tau}_{it} \leq \overline{\tau}_i < 1$, and $0 < \tau_{it} \leq \overline{\overline{\tau}}_i$.

We propose the following distributed observer for each follower.

$$\mathcal{D}^{\alpha}\Upsilon_{it} = -\mathrm{sgn}(\tilde{\Upsilon}_{it})\hat{\mathcal{M}}_i - \hat{\mu}_i\tilde{\Upsilon}_{it}, \tag{6}$$

where

$$\tilde{\Upsilon}_{it} = \sum_{j=1}^{N} a_{ij}(\Upsilon_{it} - \Upsilon_{jt}) + \sum_{k=N+1}^{N+M} a_{ik}(\hat{\Upsilon}_{it} - \nu_{kt}), \tag{7}$$

$\hat{\mathcal{M}}_i$ and $\hat{\mu}_i$ are the novel adaptive parameters, while the notation $\mathrm{sgn}(\cdot)$ represents the sign function. This observer design enables the followers to infer the necessary information about the leaders' states through the network, even in the absence of direct communication with the leaders.

Remark 1: *Consider a drone swarm where a leader drone follows a planned trajectory, and three follower drones start with different speeds and headings. Only one follower has direct access to the leader's speed, while others rely solely on neighbor communications. Through the distributed observer, each follower estimates the leader's state using local measurements and shared neighbor information. Over time, even*

indirectly connected followers refine their estimates and, under the proposed control law, adjust their speeds to match the leader, achieving complete state alignment across the swarm.

Let $\mathbf{s}_t = \left(\mathbf{s}_{1t}^T, \mathbf{s}_{2t}^T, \ldots, \mathbf{s}_{Qt}^T\right)^T$, $\Upsilon_t = \left(\Upsilon_{1t}^T, \Upsilon_{2t}^T, \ldots, \Upsilon_{Qt}^T\right)^T$, and $\nu_t = \left(\nu_{(Q+1)t}^T, \nu_{(Q+2)t}^T, \ldots, \nu_{(Q+R)t}^T\right)^T$. The systems (4)–(6) can be written in the following compact form.

$$\begin{cases} D^\alpha \mathbf{s}_t = A\mathbf{s}_t + g(\mathbf{s}_t, d_t, \tau) + \beta^F u_t + \eta^F u_{st} + \Delta, \\ D^\alpha \nu_t = \Phi(\nu_t), \\ D^\alpha \hat{\Upsilon}_t = -\operatorname{sgn}(\hat{\Upsilon}_t)\left(\hat{\mathcal{M}} \otimes I_n\right) - (\hat{\mu} \otimes I_n)\hat{\Upsilon}_t, \end{cases} \tag{8}$$

where $\hat{\mathcal{M}} = [\hat{\mathcal{M}}_1, \hat{\mathcal{M}}_2, \ldots, \hat{\mathcal{M}}_Q]^T$, $A = \operatorname{diag}(A_1, A_2, \ldots, A_Q)$, $\Delta = \operatorname{diag}(\Delta_1, \Delta_2, \ldots, \Delta_Q)$, $\operatorname{sgn}(\hat{\Upsilon}_t) = \operatorname{diag}(\operatorname{sgn}(\hat{\Upsilon}_{1t}), \ldots, \operatorname{sgn}(\hat{\Upsilon}_{Qt}))$, $\hat{\mu} = \operatorname{diag}(\hat{\mu}_1, \hat{\mu}_2, \ldots, \hat{\mu}_Q)$, $g(\mathbf{s}_t, d_t, \tau) = \left[g_1(\mathbf{s}_{1t}, d_{1t}, \tau_1), \ldots, g_Q(\mathbf{s}_{Qt}, d_{Qt}, \tau_Q)\right]^T$, and $u_t = \operatorname{diag}(u_{1t}, u_{2t}, \ldots, u_{Qt})$.

For every agent $i(t) \in \mathcal{F}_s$ the controller can be design as follows:

$$u_{it} = -\hat{\beta}_i \tilde{\varepsilon}_{it} - \hat{\Xi}_{li}\Psi_{li}(\mathbf{s}_{it}) - \hat{\Xi}_{ri}\Psi_{ri}(\mathbf{s}_{it}) - \operatorname{sgn}(\tilde{\varepsilon}_{it})\hat{\mathcal{Q}}_i - \operatorname{sgn}(\tilde{\Upsilon}_{it})\hat{\mathcal{M}}_i - \hat{\mu}_i\tilde{\Upsilon}_{it}, \quad i \in \mathcal{F}_s \tag{9}$$

where $\hat{\beta}_i$, $\hat{\mu}_i$, $\hat{\mathcal{Q}}_i$, $\hat{\mathcal{M}}_i$, $\hat{\Xi}_{li}$ and $\hat{\Xi}_{ri}$ are the undesigned adaptive parameters, and $\tilde{\varepsilon}_{it} = \mathbf{s}_{it} - \Upsilon_{it}$.

To model the uncertainty and nonlinearity in the agent dynamics, the terms $\Psi_{li}(t)$ and $\Psi_{ri}(t)$ in (9) are defined as Gaussian membership functions centered symmetrically around the origin, as follows:

$$\Psi_{li}^k(s_{ik}) = \exp\left(-\frac{(s_{ik} + a_{li}^k)^2}{2(\sigma_{li}^k)^2}\right), \quad \Psi_{ri}^k(s_{ik}) = \exp\left(-\frac{(s_{ik} + a_{ri}^k)^2}{2(\sigma_{ri}^k)^2}\right) \tag{10}$$

where k denotes the state index, and a_{li}^k, a_{ri}^k are the center offsets while σ_{li}^k, σ_{ri}^k represent the spread parameters for each fuzzy rule.

To visualise the fuzzy inference structure, Fig. 1 presents the input Gaussian membership functions $\Psi_{li}(t)$ and $\Psi_{ri}(t)$. These functions are symmetrically placed around the origin and share a common spread of $\sigma = 0.5$, thereby capturing the uncertainty in the follower agent's state $s_i(t)$.

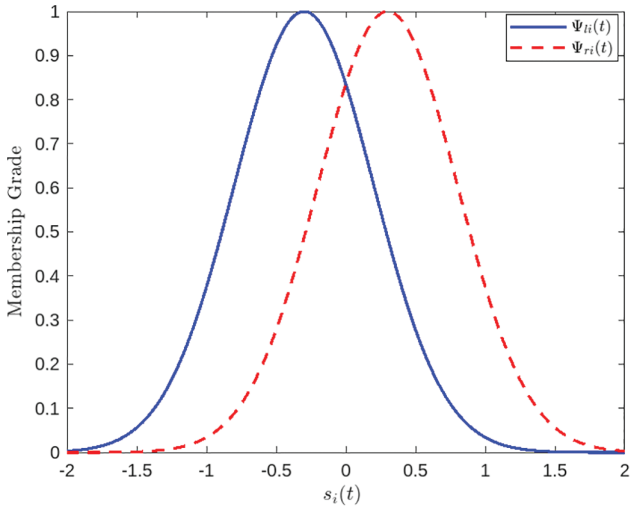

Figure 1: Gaussian membership functions $\Psi_{li}(t)$ and $\Psi_{ri}(t)$

Fig. 2 illustrates the output membership functions used in the IT-II FLS for the control signal. Five linguistic terms Negative Large (NL), Negative Small (NS), Zero (Z), Positive Small (PS),

and Positive Large (PL) are assigned to the fuzzy control output, each represented by Gaussian membership functions. To capture uncertainty, both an upper and a lower Gaussian function are defined for each linguistic term. The region bounded between these two functions forms the Footprint of Uncertainty (FOU), visually represented as a shaded area. The upper functions correspond to the overestimated interval parameter $\overline{\theta}_{i_1 i_2}$, while the lower functions relate to the underestimated interval $\underline{\theta}_{i_1 i_2}$, in accordance with the IT-II fuzzy modeling defined in Eqs. (1)–(3).

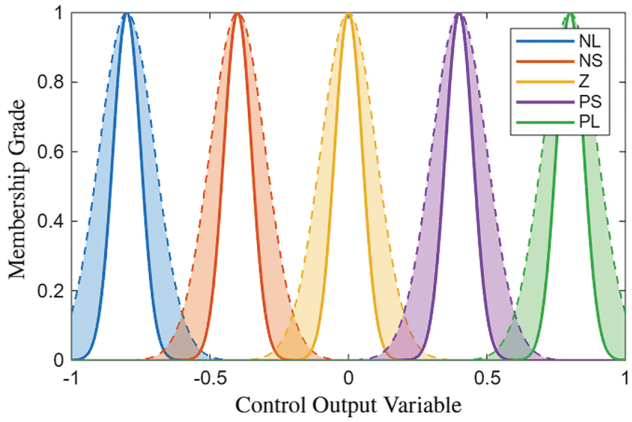

Figure 2: Gaussian membership functions $\Psi_{li}(t)$ and $\Psi_{ri}(t)$

In this paper, We are planning to devise a distributed observer (6) and controller (9) for system (4) satisfying the conditions (5), such that the system's trajectories under closed-loop control satisfy the following two conditions:

$$\lim_{t\to\infty} \operatorname{dist}(\mathbf{s}_{it}, \theta_{it}) = 0, \quad i \in \mathcal{F}_s \tag{11}$$

$$\lim_{t\to\infty} \operatorname{dist}(\theta_{it}, \mathfrak{B}) = 0, \quad i \in \mathcal{F}_s \tag{12}$$

where $\mathfrak{B} = \{\upsilon | \upsilon \in \operatorname{Co}\{\nu_{kt}, k \in \mathcal{L}_s\}\}$.

Assumption 1: *[41] From any leader to any follower, there exists a directed path that allows communication from leader to follower; however, the leader is unable to receive any feedback or information from the followers.*

Assumption 2: *[41] The unknown nonlinear functions $g_{1i}(\theta_{1t})$ and $g_{2i}(\theta_{2t})$ satisfy the Lipschitz condition:*

$$\|g_{i1}(\theta_{1t}) - g_{i1}(\theta_{2t})\| \le \rho_1 \|\theta_{1t} - \theta_{2t}\|, \quad i \in \mathcal{F}_s,$$

$$\|g_{i2}(\theta_{1t}) - g_{i2}(\theta_{2t})\| \le \rho_2 \|\theta_{1t} - \theta_{2t}\|, \quad i \in \mathcal{F}_s.$$

where ρ_1 and ρ_2 are unknown constants.

Lemma 6: *Let Assumption 1 holds, one can write the Laplacian matrix Ω as*

$$\Omega = \begin{bmatrix} \Omega_1 & \Omega_2 \\ 0_{R\times Q} & 0_{R\times R} \end{bmatrix},$$

where $\Omega_1 = \mathcal{B} - \mathcal{A} + \mathcal{D} \in \mathbb{R}^{Q\times Q}$, $\mathcal{B} = \operatorname{diag}(\mathfrak{b}_1, \mathfrak{b}_2, \ldots, \mathfrak{b}_Q)$, $\mathcal{A} = (a_{ij})_{Q\times Q}$, and $\mathcal{D} = \operatorname{diag}(d_1, d_2, \ldots, d_Q)$, also $d_i = \sum_{j=1}^{Q} a_{ij}$, $\mathfrak{b}_i = \sum_{k=Q+1}^{Q+R} a_{ik}$ and $\Omega_2 = -(a_{i,Q+K})_{Q\times R} \in \mathbb{R}^{Q\times R}$, $i, j = 1, 2, \ldots, Q$, $k = 1, 2, \ldots, R$.

The matrix Ω_1 is also invertible. In addition, every element in the matrix $-\Omega_1^{-1}\Omega_2$ is non-negative, and the sum of the elements in each row of $-\Omega_1^{-1}\Omega_2$ is equal to 1.

Lemma 7: *[33] For any vectors $\alpha, \gamma \in \mathbb{R}^n$, and for any positive κ, the following inequality holds:*

$$\alpha^T\gamma \leq \frac{\kappa}{2}\alpha^T\alpha + \frac{1}{2\kappa}\gamma^T\gamma.$$

Remark 2: *The proposed fractional Lyapunov–Krasovskii functional is designed to handle both fractional-order dynamics and mixed time-varying delays. The fractional integral terms naturally capture the system's memory effects, linking the current state with its past. The delay-dependent integral terms act as "energy storage" components that compensate for the influence of state and distributed delays. Together, these components enable the functional to absorb the effects of delays and long-memory behavior, allowing a compact dissipation inequality to be established in the subsequent stability proof.*

4 Main Results

Define the global consensus containment errors as follows:

$$\begin{cases} \tilde{\varepsilon}_t = \mathbf{s}_t - \Upsilon_t, \\ \tilde{\Upsilon}_t = (\Omega_1 \otimes I_n)\,\Upsilon_t + (\Omega_2 \otimes I_n)\,v_t. \end{cases} \tag{13}$$

If $\lim_{t\to+\infty}\tilde{\varepsilon}_t = 0$ and $\lim_{t\to+\infty}\tilde{\Upsilon}_t = 0$ are satisfied, then Eqs. (11) and (12) are also valid.

Now, from (8), differentiating both sides of Eq. (13) gives.

$$\begin{cases} \mathcal{D}^a\tilde{\varepsilon}_t = A\mathbf{s}_t + g(\mathbf{s}_t, d_t, \tau_t) + \beta^F u_t + \eta^F u_{st} + \Delta_t + \operatorname{sgn}(\tilde{\Upsilon}_t)\left(\hat{\mathcal{M}} \otimes I_n\right) + \left(\hat{\mu} \otimes I_n\right)\hat{\Upsilon}_t, \\ \mathcal{D}^a\tilde{\Upsilon}_t = (\Omega_1 \otimes I_n)\left(-\operatorname{sgn}(\tilde{\Upsilon}_t)\left(\hat{\mathcal{M}} \otimes I_n\right) - \left(\hat{\mu} \otimes I_n\right)\tilde{\Upsilon}_t + \left(\Omega_1^{-1}\Omega_2 \otimes I_n\right)\Phi(v_t)\right) \end{cases} \tag{14}$$

The CC problem examined in this paper can be reformulated as an asymptotic stabilization problem for Eq. (14).

Remark 3: *The proposed controller and observer contain several adaptive and fuzzy tuning parameters, including $\gamma_{1i}, \ldots, \gamma_{8i}$ and the spread/center values of the Gaussian membership functions. These parameters influence convergence speed, robustness, and control smoothness. In general, larger adaptive gains accelerate convergence but may increase transient oscillations, while smaller gains ensure smoother response at the cost of slower adaptation. The Gaussian membership functions are chosen to cover the expected range of the state variables, with moderate overlap to balance accuracy and robustness.*

Theorem 1: *Considering the system (14) and under Assumptions 1 and 2, if positive definite $P \in \mathbb{R}^{n\times n}$ and symmetric matrix exists that satisfies $P\Omega_1 + \Omega_1^T P = I$, then it is possible to design a distributed observer (6), an adaptive controller (9), and parameter adaptation rates (15) such that the system achieves asymptotic stability, i.e.*

$$\lim_{t\to\infty}\tilde{\mathbf{s}}_{it} = 0, \quad \lim_{t\to\infty}\tilde{\Upsilon}_{it} = 0.$$

We define the adaptive rates as follows:

$$\mathcal{D}^{\alpha}\hat{\beta}_i = \gamma_{7i}\tilde{\varepsilon}_{it}^{T}\tilde{\varepsilon}_{it},$$
$$\mathcal{D}^{\alpha}\hat{\mu}_i = \gamma_{8i}\tilde{\Upsilon}_{it}^{T}\tilde{\Upsilon}_{it},$$
$$\mathcal{D}^{\alpha}\hat{\Xi}_{li} = Proj\left(\hat{\Xi}_{li}, \gamma_{5i}\Psi_{li}(\mathbf{s}_{it})\tilde{\varepsilon}_{it}^{T}\right),$$
$$\mathcal{D}^{\alpha}\hat{\Xi}_{ri} = Proj\left(\hat{\Xi}_{ri}, \gamma_{6i}\Psi_{ri}(\mathbf{s}_{it})\tilde{\varepsilon}_{it}^{T}\right),$$
$$\mathcal{D}^{\alpha}\hat{\mathcal{N}}_i = \gamma_{3i}sgn(\tilde{\varepsilon}_{it}^{T})\tilde{\varepsilon}_{it},$$
$$\mathcal{D}^{\alpha}\hat{\mathcal{M}}_i = \gamma_{4i}sgn(\tilde{\Upsilon}_{it}^{T})\tilde{\Upsilon}_{it}. \tag{15}$$

The projection operator is defined as:

$$Proj(\xi_1, \xi_2) = \begin{cases} \xi_2 - \varpi\xi_2 g(\xi_1), & if\ g(\xi_1) > 0\ and\ \xi_2^{T}\nabla g(\xi_1) > 0, \\ \xi_2, & otherwise, \end{cases} \tag{16}$$

with

$$\varpi = \frac{\nabla g(\xi_1)\left(\nabla g(\xi_1)\right)^{T}}{\|\nabla g(\xi_1)\|^2}, \quad g(\xi_1) = \frac{\|\xi_1\|^2 - \xi_M^2}{\epsilon_{\xi}\xi_M^2}. \tag{17}$$

where ξ_M defines a boundary, and ϵ_{ξ} represents a specified boundary tolerance. $\hat{\beta}_i$ and $\hat{\mu}_i$ are approximations of β_i and μ_i, respectively, where

$$\beta_i = \|A_i\| + \frac{1}{2}\kappa_{1i}\|A_i\|^2 + \frac{1}{2}(\kappa_{2i} + \kappa_{3i} + \kappa_{4i} + \kappa_{5i}) + \gamma_{1i}\rho_{i1}^2 + \gamma_{2i}\rho_{i2}^2 + \epsilon_{1i},$$
$$\mu_i = \frac{\Omega_M}{2\kappa_{1i}} + \gamma_{1i}\rho_{i1}^2\Omega_M + \gamma_{2i}\overline{\overline{\tau}}_i\rho_{i2}^2\Omega_M + \epsilon_{2i}, \quad i \in \mathcal{F}_s. \tag{18}$$

The following conditions must be met by other parameters:

$$2\gamma_{1i}(1 - \overline{d}_i) \geq \kappa_{2i}^{-1}, \quad i \in \mathcal{F}_s,$$
$$2\gamma_{1i}(1 - \overline{d}_i) \geq \kappa_{3i}^{-1}, \quad i \in \mathcal{F}_s,$$
$$2\gamma_{2i}(1 - \overline{\tau}_i) \geq \overline{\overline{\tau}}_i\kappa_{4i}^{-1}, \quad i \in \mathcal{F}_s,$$
$$2\gamma_{2i}(1 - \overline{\tau}_i) \geq \overline{\overline{\tau}}_i\kappa_{5i}^{-1}, \quad i \in \mathcal{F}_s. \tag{19}$$

Proof: We have

$$\begin{aligned} g_i(\mathbf{s}_{it}, d_{it}, \tau_{it}) &= g_{1i}\mathbf{s}_{i(t-d_{it})} + \int_{t-\tau_{it}}^{t} g_{2i}(\mathbf{s}_{is})\,ds + g_{3i}(\mathbf{s}_{it}) \\ &= \delta_{\tilde{\mathbf{s}}_{i(t-d_{it})}} + \delta_{\tilde{\Upsilon}_{i(t-d_{it})}} + \int_{t-\tau_{it}}^{t}\left(\eta_{\tilde{\mathbf{s}}_{is}} + \eta_{\tilde{\Upsilon}_{is}}\right)ds + \Xi_{li}^{*T}\Psi_{li}(\mathbf{s}_{it}) + \Xi_{ri}^{*T}\Psi_{ri}(\mathbf{s}_{it}) + \mathfrak{O}_{1it} \end{aligned} \tag{20}$$

where $\delta_{\tilde{\mathbf{s}}_{it}} = g_{1i}(\mathbf{s}_{it}) - g_{1i}(\Upsilon_{it})$, $\eta_{\tilde{\mathbf{s}}_{it}} = g_{2i}(\mathbf{s}_{it}) - g_{2i}(\Upsilon_{it})$, $\delta_{\tilde{\Upsilon}_{it}} = g_{1i}(\Upsilon_{it}) - g_{1i}\left(\sum_{j=Q+1}^{Q+R}\xi_{ij}\Phi_k(\nu_{kt})\right)$, $\eta_{\tilde{\Upsilon}_{it}} = g_{2i}(\Upsilon_{it}) - g_{2i}\left(\sum_{j=Q+1}^{Q+R}\xi_{ij}\Phi_k(\nu_{kt})\right)$, $\mathfrak{O}_{1it} = g_{1i}\left(\sum_{j=Q+1}^{Q+R}\xi_{ij}\Phi_k\left(\nu_{k(t-d_{it})}\right)\right) + \int_{t-\tau_{it}}^{t} g_{2i}\left(\sum_{j=Q+1}^{Q+R}\xi_{ij}\Phi_k(\nu_{ks})\right)ds + \epsilon_{it}$,

where ϵ_{it} is the approximation error satisfying the condition $\|\epsilon_{it}\| \leq \overline{\epsilon}_i$ with $\overline{\epsilon}_i$ an unknown bounded constant.

Furthermore, Ξ_{li}^* and Ξ_{ri}^* satisfy

$$[\Xi_{li}^*, \Xi_{ri}^*] = \arg\min_{\Xi_{li},\Xi_{ri}} \left[\sup_{\mathbf{s}_i} \left| g_{3i}(\mathbf{s}_i) - \Xi_{li}^T \Psi_{li}(x_i) - \Xi_{ri}^T \Psi_{ri}(\mathbf{s}_i) \right| \right] \tag{21}$$

To study the system's stability, we proceed by formulating the following Lyapunov-Krasovskii functional.

$$V_t = V_{1t} + V_{2t} + V_{3t} + V_{4t},$$

where

$$V_{1t} = D^{\alpha-1}\left(\frac{1}{2}\tilde{\varepsilon}_t^T\tilde{\varepsilon}_t + \tilde{\Upsilon}_t^T(P \otimes I_n)\tilde{\Upsilon}_t\right),$$

$$V_{2t} = \sum_{i=1}^{Q}\left(\gamma_{1i}\int_{t-d_{it}}^{t}\left(\delta_{\tilde{\varepsilon}_{is}}^T\delta_{\tilde{\varepsilon}_{is}} + \delta_{\tilde{\Upsilon}_{is}}^T\delta_{\tilde{\Upsilon}_{is}}\right)ds\right) + \sum_{i=1}^{Q}\left(\gamma_{2i}\int_{t-\tau_{it}}^{t}\int_{v}^{t}\left(\eta_{\tilde{\varepsilon}_{is}}^T\eta_{\tilde{\varepsilon}_{is}} + \eta_{\tilde{\Upsilon}_{is}}^T\eta_{\tilde{\Upsilon}_{is}}\right)ds\,dv\right),$$

$$V_{3t} = \sum_{i=1}^{Q} D^{\alpha-1}\left(\frac{1}{2\gamma_{3i}}\tilde{\mathcal{Q}}_i^2 + \frac{1}{2\gamma_{4i}}\tilde{\mathcal{M}}_i^2\right) + \sum_{i=1}^{Q} D^{\alpha-1}\left(\mathrm{Tr}\left\{\frac{1}{2\gamma_{5i}}\tilde{\Xi}_{li}^T\tilde{\Xi}_{li} + \frac{1}{2\gamma_{6i}}\tilde{\Xi}_{ri}^T\tilde{\Xi}_{ri}\right\}\right),$$

$$V_{4t} = \sum_{i=1}^{Q} D^{\alpha-1}\left(\frac{1}{2\gamma_{7i}}\tilde{\beta}_i^2 + \frac{1}{2\gamma_{8i}}\tilde{\mu}_i^2\right) \tag{22}$$

Here $\tilde{\mathcal{Q}}_i$ denotes the estimation error of the adaptive parameter Q_i, defined as

$$\tilde{\mathcal{Q}}_i = \mathcal{Q}_i - \mathcal{Q}_i^*,$$

where Q_i^* represents the ideal value of the adaptive gain that exactly compensates the corresponding uncertainty.

By differentiating $V_1(t)$ and applying Lemma 1 along with the condition $P\Omega_1 + \Omega_1^T P = I$, we can derive the following result:

$$\begin{aligned}\frac{dV_{1t}}{dt} \leq{}& \sum_{i=1}^{Q}\tilde{\varepsilon}_{it}^T\left(A_i\mathbf{s}_{it} + g_i(\mathbf{s}_{it}, d_{it}, \tau_{it}) + \overline{\beta}^F u_{it}\right) \\ &+ \sum_{i=1}^{Q}\tilde{\varepsilon}_{it}^T\left(\Delta_i + \mathrm{sgn}(\tilde{\gamma}_{it})\hat{M}_i + \hat{\mu}_i\tilde{\Upsilon}_t + \overline{\eta}^F u_{si}\right) \\ &- \sum_{i=1}^{Q}\left(\hat{\mu}_i\tilde{\Upsilon}_{it}^T\tilde{\Upsilon}_{it} + \tilde{\Upsilon}_{it}^T\mathrm{sgn}(\tilde{\Upsilon}_{it})\hat{M}_i + \tilde{\Upsilon}_{it}^T\sum_{k=Q+1}^{Q+R}\xi_{ik}\Phi_k(\nu_{kt})\right)\end{aligned} \tag{23}$$

Let

$$e_{it} = \Upsilon_{it} - \sum_{k=Q+1}^{Q+R}\xi_{ik}\nu_{kt}. \tag{24}$$

Taking into account Eq. (16) and performing straightforward manipulations, we can arrive at the following expression:

$$\begin{aligned}\frac{d\mathcal{V}_{1t}}{dt} \leq & \sum_{i=1}^{Q} \tilde{\varepsilon}_{it}^{T}\left(A_i(\tilde{\varepsilon}_{it}+e_{it})+\Xi_{li}^{*}\Psi_{li}(\mathbf{s}_{it})+\Xi_{ri}^{*}\Psi_{ri}(\mathbf{s}_{it})\right)\\ & +\sum_{i=1}^{Q}\tilde{\varepsilon}_{it}^{T}\left(\delta_{\tilde{\varepsilon}_{i(t-d_{it})}}+\delta_{\tilde{\Upsilon}_{i(t-d_{it})}}+\overline{\beta}^{F}u_{it}+\eta_i^{F}u_{si}+\hat{\mu}_i\tilde{\Upsilon}_{it}+\mathfrak{D}_i\right)\\ & +\sum_{i=1}^{N}\tilde{\varepsilon}_{it}^{T}\left(\int_{t-\tau_{it}}^{t}\left(\eta_{\tilde{\varepsilon}_{is}}+\eta_{\tilde{\Upsilon}_{is}}\right)ds+\operatorname{sgn}(\tilde{\Upsilon}_{it})\hat{\mathcal{M}}_i\right)+\\ & \sum_{i=1}^{Q}\tilde{\Upsilon}_{it}^{T}\left(-\operatorname{sgn}(\tilde{\Upsilon}_{it})\hat{\mathcal{M}}_i-\hat{\mu}_i\tilde{\Upsilon}_{it}-\sum_{k=Q+1}^{Q+R}\xi_{ik}\Phi_k(\nu_{kt})\right).\end{aligned} \tag{25}$$

where $\mathfrak{D}_i=\mathfrak{D}_{1it}+\Delta_i+A_i\sum_{k=Q+1}^{Q+R}\xi_{ik}\nu_{kt}$.

Given that the states of the leaders are bounded and $\sum_{k=Q+1}^{Q+R}\xi_{ik}=1$ for $\forall i\in\mathcal{F}_s$,we can determine $\mathcal{N}_i$ and $\mathcal{M}_i$ such that the following equations are satisfied:

$$\|\mathcal{D}_i\|\leq\mathcal{N}_i,\quad i\in\mathcal{F}_s, \tag{26}$$

$$\left\|\sum_{k=Q+1}^{Q+R}\xi_{ik}\Phi_k(\nu_{kt})\right\|\leq\mathcal{M}_i,\quad i\in\mathcal{F}_s. \tag{27}$$

By substituting (5) into inequality (25) and by using inequalities (26) and (27), we can derive:

$$\begin{aligned}\frac{d\mathcal{V}_{1t}}{dt}\leq & \sum_{i=1}^{Q}\tilde{\varepsilon}_{it}^{T}\big(A_i(\tilde{\varepsilon}_{it}+e_{it})-\tilde{\Xi}_{li}^{T}\Psi_{li}(\mathbf{s}_{it})-\tilde{\Xi}_{ri}^{T}\Psi_{ri}(\mathbf{s}_{it})+\delta_{\tilde{\varepsilon}_{i(t-d_{it})}}+\delta_{\tilde{\Upsilon}_{i(t-d_{it})}}-\hat{\beta}_i\overline{\beta}^{F}\tilde{\varepsilon}_{it}\\ & +\int_{t-\tau_{it}}^{t}(\eta_{\tilde{\varepsilon}_{is}}+\eta_{\tilde{\Upsilon}_{is}})ds-\overline{\beta}^{F}\operatorname{sgn}(\tilde{\varepsilon}_{it})\tilde{\mathcal{N}}_i\big)+\sum_{i=1}^{Q}\tilde{\Upsilon}_{it}^{T}\left(-\operatorname{sgn}(\tilde{\Upsilon}_{it})\tilde{\mathcal{M}}_i-\hat{\mu}_i\tilde{\Upsilon}_{it}\right).\end{aligned} \tag{28}$$

According to the definitions of e_{it} and Υ_{it}, we can obtain

$$\sum_{i=1}^{Q}e_{it}^{T}e_{it}=e_t^{T}e_t=\tilde{\Upsilon}_t^{T}(\Omega_1^{-T}\Omega_1^{-1}\otimes I_n)\tilde{\Upsilon}_t\leq\Omega_M\tilde{\Upsilon}_t^{T}\tilde{\Upsilon}_t=\Omega_M\sum_{i=1}^{Q}\tilde{\Upsilon}_{it}^{T}\tilde{\Upsilon}_{it}, \tag{29}$$

where Ω_M is greater than or equal to the maximum eigenvalue of matrix $\Omega_1^{-T}\Omega_1^{-1}$.

Using Lemma 7 in (28), we have:

$$\sum_{i=1}^{Q}\tilde{\mathbf{s}}_{it}^{T}A_ie_{it}\leq\sum_{i=1}^{Q}\left(\frac{\kappa_{1i}\|A_i\|^2}{2}\tilde{\mathbf{s}}_{it}^{T}\tilde{\mathbf{s}}_{it}+\frac{\Omega_M}{2\kappa_{1i}}\tilde{\Upsilon}_{it}^{T}\tilde{\Upsilon}_{it}\right),$$

$$\sum_{i=1}^{Q}\tilde{\mathbf{s}}_{it}^{T}\delta_{\tilde{\mathbf{s}}_i(t-d_{it})}\leq\sum_{i=1}^{Q}\left(\frac{\kappa_{2i}}{2}\tilde{\mathbf{s}}_{it}^{T}\tilde{\mathbf{s}}_{it}+\frac{1}{2\kappa_{2i}}\delta\tilde{\mathbf{s}}_{i(t-d_{it})}^{T}\delta\tilde{\mathbf{s}}_{i(t-d_{it})}\right),$$

$$\sum_{i=1}^{Q}\tilde{\mathbf{s}}_{it}^{T}\delta\tilde{\Upsilon}_{i(t-d_{it})}\leq\sum_{i=1}^{Q}\left(\frac{\kappa_{3i}}{2}\tilde{\mathbf{s}}_{it}^{T}\tilde{\mathbf{s}}_{it}+\frac{1}{2\kappa_{3i}}\delta\tilde{\Upsilon}_{i(t-d_{it})}^{T}\delta\tilde{\Upsilon}_{i(t-d_{it})}\right),$$

$$\sum_{i=1}^{Q}\tilde{\mathbf{s}}_{it}^{T}\left(\int_{t-\tau_{it}}^{t}\eta_{\tilde{\mathbf{s}}_{is}}\,ds\right)\leq\sum_{i=1}^{Q}\left(\frac{\kappa_{4i}}{2}\tilde{\mathbf{s}}_{it}^{T}\tilde{\mathbf{s}}_{it}+\frac{1}{2\kappa_{4i}}\left(\int_{t-\tau_{it}}^{t}\eta_{\tilde{\mathbf{s}}_{is}}\,ds\right)^{T}\left(\int_{t-\tau_{it}}^{t}\eta_{\tilde{\mathbf{s}}_{is}}\,ds\right)\right),$$

$$\sum_{i=1}^{Q}\tilde{\mathbf{s}}_{it}^{T}\left(\int_{t-\tau_{it}}^{t}\eta_{\tilde{\Upsilon}_{is}}\,ds\right)\leq\sum_{i=1}^{Q}\left(\frac{\kappa_{5i}}{2}\tilde{\mathbf{s}}_{it}^{T}\tilde{\mathbf{s}}_{it}+\frac{1}{2\kappa_{5i}}\left(\int_{t-\tau_{it}}^{t}\eta_{\tilde{\Upsilon}_{is}}\,ds\right)^{T}\left(\int_{t-\tau_{it}}^{t}\eta_{\tilde{\Upsilon}_{is}}\,ds\right)\right). \tag{30}$$

By differentiating $V_2(t)$, and taking into account Lemma 2 along with the pertinent conditions for time-delay compliance, the desired result can be achieved:

$$\begin{aligned}\frac{dV_2(t)}{dt}\leq&\sum_{i=1}^{Q}\left(\gamma_{1i}\delta_{\tilde{\mathbf{s}}_i(t)}^{T}\delta_{\tilde{\mathbf{s}}_i(t)}-\gamma_{1i}\left(1-\overline{d}_{it}\right)\delta_{\tilde{\mathbf{s}}_i(t-d_{it})}^{T}\delta_{\tilde{\mathbf{s}}_i(t-d_{it})}\right)+\sum_{i=1}^{Q}\left(\gamma_{1i}\delta_{\tilde{\Upsilon}_{it}}^{T}\delta_{\tilde{\Upsilon}_{it}}-\gamma_{1i}\left(1-\overline{d}_{i}(t)\right)\delta_{\tilde{\Upsilon}_{i(t-d_{it})}}^{T}\delta_{\tilde{\Upsilon}_{i(t-d_{it})}}\right)\\&+\sum_{i=1}^{Q}\left(\gamma_{2i}\overline{\overline{\tau}}_{i}\eta_{\tilde{\mathbf{s}}_i(t)}^{T}\eta_{\tilde{\mathbf{s}}_i(t)}+\gamma_{2i}\overline{\overline{\tau}}_{i}\eta_{\tilde{\Upsilon}_i(t)}^{T}\eta_{\tilde{\Upsilon}_i(t)}\right)-\sum_{i=1}^{Q}\left(\gamma_{2i}(1-\overline{\tau}_{i})\overline{\overline{\tau}}_{i}^{-1}\left(\int_{t-\tau_i(t)}^{t}\eta_{\tilde{\mathbf{s}}_{is}}ds\right)^{T}\left(\int_{t-\tau_i(t)}^{t}\eta_{\tilde{\mathbf{s}}_{is}}ds\right)\right)\\&-\sum_{i=1}^{Q}\left(\gamma_{2i}(1-\overline{\tau}_{i})\overline{\overline{\tau}}_{i}^{-1}\left(\int_{t-\tau_i(t)}^{t}\eta_{\tilde{\Upsilon}_{is}}ds\right)^{T}\left(\int_{t-\tau_i(t)}^{t}\eta_{\tilde{\Upsilon}_{is}}ds\right)\right)\end{aligned} \tag{31}$$

By using definitions of $\delta_{\tilde{\varepsilon}_{it}}$, $\delta_{\tilde{\Upsilon}_{it}}$, $\eta_{\tilde{\varepsilon}_{it}}$, and $\eta_{\tilde{\Upsilon}_{it}}$ and Assumption 2, we can get the following relationships:

$$\gamma_{1i}\delta_{\tilde{\varepsilon}_{it}}^{T}\delta_{\tilde{\varepsilon}_{it}}\leq\gamma_{1i}\rho_{1i}^{2}\tilde{\mathbf{s}}_{it}^{T}\tilde{\mathbf{s}}_{it}, \tag{32}$$

$$\sum_{i=1}^{Q}\gamma_{1i}\delta_{\tilde{\Upsilon}_{it}}^{T}\delta_{\tilde{\Upsilon}_{it}}\leq\sum_{i=1}^{Q}\gamma_{1i}\rho_{1i}^{2}e_{it}^{T}e_{it}\leq\sum_{i=1}^{Q}\gamma_{1i}\rho_{1i}^{2}\Omega_{M}\tilde{\Upsilon}_{it}^{T}\tilde{\Upsilon}_{it}, \tag{33}$$

$$\gamma_{2i}\tau_{i}\eta_{\tilde{\varepsilon}_{it}}^{T}\eta_{\tilde{\varepsilon}_{it}}\leq\gamma_{2i}\rho_{2i}^{2}\tilde{\mathbf{s}}_{it}^{T}\tilde{\mathbf{s}}_{it}, \tag{34}$$

$$\sum_{i=1}^{Q}\gamma_{2i}\overline{\overline{\tau}}_{i}\eta_{\tilde{\Upsilon}_{it}}^{T}\eta_{\tilde{\Upsilon}_{it}}\leq\sum_{i=1}^{Q}\gamma_{2i}\overline{\overline{\tau}}_{i}\rho_{2i}^{2}e_{it}^{T}e_{it}\leq\sum_{i=1}^{Q}\gamma_{2i}\overline{\overline{\tau}}_{i}\rho_{2i}^{2}\Omega_{M}\tilde{\Upsilon}_{it}^{T}\tilde{\Upsilon}_{it}. \tag{35}$$

Using inequalities (28)–(31), we can derive the following result:

$$\begin{aligned}\frac{d\mathcal{V}_1(t)}{dt}+\frac{d\mathcal{V}_2(t)}{dt}\leq&\sum_{i=1}^{Q}\left(-\epsilon_{1i}\tilde{\mathbf{s}}_{it}^{T}\tilde{\mathbf{s}}_{it}-\epsilon_{2i}\tilde{\Upsilon}_{it}^{T}\tilde{\Upsilon}_{it}\right)+\sum_{i=1}^{Q}\left(-\tilde{\beta}_{i}\tilde{\mathbf{s}}_{it}^{T}\tilde{\mathbf{s}}_{it}-\tilde{\mu}_{i}\tilde{\Upsilon}_{it}^{T}\tilde{\Upsilon}_{it}\right)\\&+\sum_{i=1}^{Q}\tilde{\mathbf{s}}_{it}^{T}\left(-\tilde{\Xi}_{li}^{T}\Psi_{li}(\mathbf{s}_{it})-\tilde{\Xi}_{ri}^{T}\Psi_{ri}(\mathbf{s}_{it})\right)+\sum_{i=1}^{Q}\left(-\overline{\beta}^{F}\operatorname{sgn}(\tilde{\mathbf{s}}_{it}^{T})\tilde{\mathcal{N}}_{i}\tilde{\mathbf{s}}_{it}-\operatorname{sgn}(\tilde{\Upsilon}_{it}^{T})\tilde{\mathcal{M}}_{i}\tilde{\Upsilon}_{it}\right).\end{aligned} \tag{36}$$

By evaluating the derivative of $\mathcal{V}_{3t}$ and $\mathcal{V}_{4t}$,we obtain the following:

$$\frac{d\mathcal{V}_{3t}}{dt}\leq\sum_{i=1}^{Q}\left(\frac{1}{\gamma_{3i}}\tilde{\mathcal{N}}_{i}\mathcal{D}^{\alpha}\hat{\mathcal{N}}_{i}+\frac{1}{\gamma_{4i}}\tilde{\mathcal{M}}_{i}\mathcal{D}^{\alpha}\hat{\mathcal{M}}_{i}\right)+\sum_{i=1}^{Q}\operatorname{Tr}\left\{\frac{1}{\gamma_{5i}}\tilde{\Xi}_{li}^{T}\mathcal{D}^{\alpha}\hat{\Xi}_{li}+\frac{1}{\gamma_{6i}}\tilde{\Xi}_{ri}^{T}\mathcal{D}^{\alpha}\hat{\Xi}_{ri}\right\}, \tag{37}$$

$$\frac{d\mathcal{V}_{4t}}{dt} \leq \sum_{i=1}^{Q} \left(\frac{1}{\gamma_{7i}} \tilde{\beta}_i \mathcal{D}^{\alpha} \hat{\beta}_i + \frac{1}{\gamma_{8i}} \tilde{\mu}_i \mathcal{D}^{\alpha} \hat{\mu}_i \right). \tag{38}$$

By taking into account (36)–(38), we can derive the following:

$$\frac{d\mathcal{V}_t}{dt} \leq \sum_{i=1}^{Q} \left(-\epsilon_{1i} \tilde{\mathbf{s}}_{it}^T \tilde{\mathbf{s}}_{it} - \epsilon_{2i} \tilde{\Upsilon}_{it}^T \tilde{\Upsilon}_{it} \right). \tag{39}$$

Taking the integral of both sides of inequality (39) yields

$$\mathcal{V}(T) - \mathcal{V}(0) \leq \int_0^T \left(-\epsilon_{1i} \tilde{\mathbf{s}}_{it}^T \tilde{\mathbf{s}}_{it} - \epsilon_{2i} \tilde{\Upsilon}_{it}^T \tilde{\Upsilon}_{it} \right) dt.$$

Therefore,

$$\int_0^T \epsilon_{1i} \tilde{\mathbf{s}}_{it}^T \tilde{\mathbf{s}}_{it}\, dt + \int_0^T \epsilon_{2i} \tilde{\Upsilon}_{it}^T \tilde{\Upsilon}_{it}\, dt \leq \mathcal{V}(0)$$

When $T \to \infty$, the right hand side of above inequality is bounded, so the left-hand side is also bounded. Therefore, $\mathcal{V}(t)$ is bounded, and $\lim_{T\to\infty} \int_0^T \left(\epsilon_{1i} \tilde{\mathbf{s}}_{it}^T \tilde{\mathbf{s}}_{it} + \epsilon_{2i} \tilde{\Upsilon}_{it}^T \tilde{\Upsilon}_{it} \right) dt$ is bounded.

According to Lemma 5, we can then obtain

$$\lim_{t\to\infty} \left(\epsilon_{1i} \tilde{\mathbf{s}}_{it}^T \tilde{\mathbf{s}}_{it} + \epsilon_{2i} \tilde{\Upsilon}_{it}^T \tilde{\Upsilon}_{it} \right) = 0.$$

Thus, we can arrive at:

$$\lim_{t\to\infty} \tilde{\mathbf{s}}_{it} = 0, \quad \lim_{t\to\infty} \tilde{\Upsilon}_{it} = 0.$$

Therefore, the theorem is established. □

5 Simulation

5.1 Simulation Work

Consider a MAS with two leaders and five followers, where the leader's dynamics are described by the FO Lorenz system shown in Fig. 3. The x-axis, y-axis, and z-axis represent the first (ν_{i1}), second (ν_{i2}), and third (ν_{i3}) state variables of Leaders $i = 6, 7$, respectively. The FO Lorenz system introduces a memory effect and fractional calculus into the classical Lorenz system, making it more suitable for modeling complex systems with long-term dependencies. The equations governing the system's behavior can be expressed as follows:

$$\begin{cases} D^{0.85}\nu_{i1}(t) = 10\left(\nu_{i2}(t) - \nu_{i1}(t)\right), \\ D^{0.85}\nu_{i2}(t) = 28\nu_{i1}(t) - \nu_{i2}(t) - \nu_{i1}(t)\nu_{i3}(t), \\ D^{0.85}\nu_{i3}(t) = \nu_{i1}(t)\nu_{i2}(t) - \frac{8}{3}\nu_{i3}(t), \quad i = 6, 7. \end{cases} \tag{40}$$

where $D^{0.85}$ denotes the fractional derivative of order 0.85. The Lorenz system, a classical chaotic system, is adopted to define the dynamics of the leaders. Its nonlinear and sensitive behavior serves to rigorously test the performance of the proposed control scheme. By introducing a leader with fractional-order chaotic dynamics, we aim to simulate realistic and unpredictable conditions under which a robust containment control strategy must operate effectively.

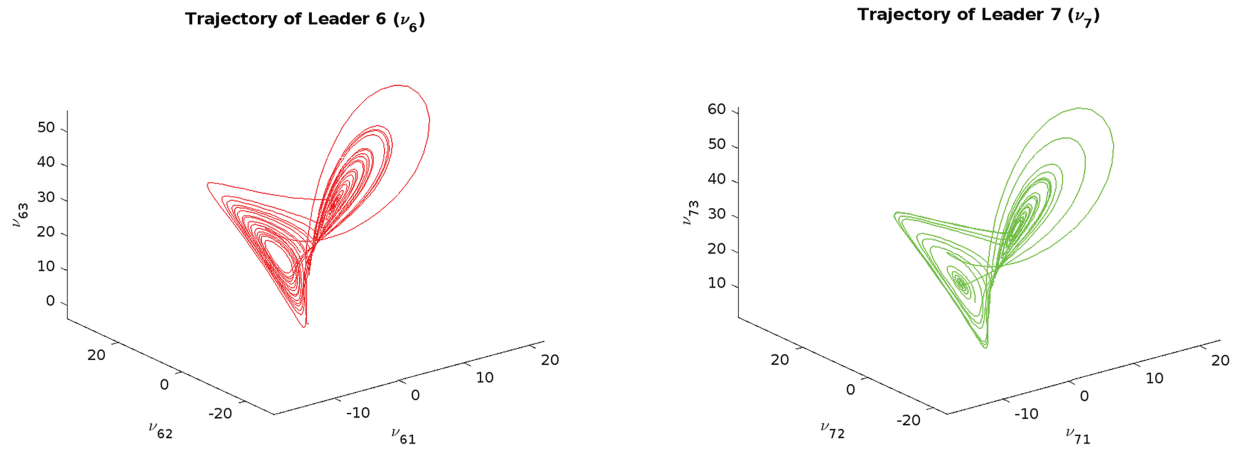

Figure 3: Trajectory of the phase plane for FO Lorenz system (40)

The dynamic equation of the followers and relevant parameters are described as follows:

$$A_i = \begin{bmatrix} 0 & -1 & 0 \\ 1 & 1 & 0 \\ 0 & 0 & -5 \end{bmatrix}, \quad g_{i3}(\mathbf{s}_{it}) = \begin{bmatrix} \mathbf{s}^2 \\ 0 \\ 0 \end{bmatrix}$$

$$g_{11}(\mathbf{s}_{1(t-d_{1t})}) = \begin{bmatrix} \sin(\mathbf{s}_{11(t-d_{1t})}) \\ \mathbf{s}_{12(t-d_{1t})} \\ \mathbf{s}^2_{13(t-d_{1t})} \end{bmatrix}, \quad d_{1t} = 0.5\sin^2(t)$$

$$g_{12}(\mathbf{s}_{1t}) = \begin{bmatrix} e^{-\mathbf{s}_{11t}} \\ \cos(\mathbf{s}_{12t}) \\ \mathbf{s}_{13t} \end{bmatrix}, \quad \tau_{1t} = 0.3\cos(t),$$

$$g_{21}(\mathbf{s}_2(t-d_{2t})) = \begin{bmatrix} \cos(\mathbf{s}_{21(t-d_{2t})}) \\ \mathbf{s}_{22(t-d_{2t})} \\ \mathbf{s}_{23(t-d_{2t})} \end{bmatrix}, \quad d_{2t} = 0.4\cos^2(t)$$

$$g_{22}(\mathbf{s}_{2t}) = \begin{bmatrix} \mathbf{s}^2_{21t} \\ e^{-\mathbf{s}_{22t}} \\ \sin(\mathbf{s}_{23t}) \end{bmatrix} \quad \tau_{2t} = 0.5\sin(t)$$

$$g_{31}(\mathbf{s}_3(t-d_{3t})) = \begin{bmatrix} \mathbf{s}_{31(t-d_{3t})} \\ \sin(\mathbf{s}_{32(t-d_{3t})}) \\ \mathbf{s}_{33(t-d_{3t})} \end{bmatrix} \quad d_{3t} = 0.3e^{-t}$$

$$g_{32}(\mathbf{s}_{3t}) = \begin{bmatrix} e^{-\mathbf{s}_{31t}} \\ \mathbf{s}_{32t} \\ \cos(\mathbf{s}_{33t}) \end{bmatrix} \quad \tau_{3t} = 0.2\sin(t)$$

$$g_{41}(\mathbf{s}_{4(t-d_{4t})}) = \begin{bmatrix} \mathbf{s}^2_{41(t-d_{4t})} - d_{4t} \\ \sin(\mathbf{s}_{42(t-d_{4t})}) \\ \log(1+\mathbf{s}_{43(t-d_{4t})}) \end{bmatrix} \quad d_{4t} = 0.3\cos^2(t)$$

$$g_{42}(\mathbf{s}_{4t}) = \begin{bmatrix} e^{\mathbf{s}_{41t}} \\ \mathbf{s}_{42t} \\ \cos(\mathbf{s}_{43t}) \end{bmatrix} \quad \tau_{4t} = 0.2e^{-t}$$

$$g_{51}(\mathbf{s}_{5(t-d_{5t})}) = \begin{bmatrix} \sin(\mathbf{s}_{51(t-d_{5t})} \\ \mathbf{s}_{52(t-d_{5t})} \\ \cos(\mathbf{s}_{53(t-d_{5t})} \end{bmatrix} \quad d_{5t} = 0.2\sin^2(t)$$

$$g_{52}(\mathbf{s}_{5t}) = \begin{bmatrix} \mathbf{s}_{51t}^3 \\ e^{-\mathbf{s}_{52t}} \\ \mathbf{s}_{53t} \end{bmatrix} \quad \tau_{5t} = 0.4e^{-t}$$

$$\Delta_{1t} = \tanh(\mathbf{s}_{1t}) + \left[\cos(2t), \sin(2t), 0\right]^T, \quad \Delta_{2t} = 6\sin(3\mathbf{s}_{2t}),$$

$$\Delta_{3t} = 0.7\sin(2.5\mathbf{s}_3(t)) + \left[0.2, -0.3, 0.02\right]^T,$$

$$\Delta_{4t} = \left[\cos^3(\mathbf{s}_{41t}), \cos^3(\mathbf{s}_{42t}), \cos^3(\mathbf{s}_{43t})\right]^T,$$

$$\Delta_{5t} = \left[\cos(3\mathbf{s}_{51t})\sin(\mathbf{s}_{51t}), \cos(3\mathbf{s}_{52t})\sin(\mathbf{s}_{52t}), \cos(3\mathbf{s}_{53t})\sin(\mathbf{s}_{53t})\right]^T$$

Setting $0.55 = \beta_i^F \leq \beta_i^F \leq \overline{\beta}_i^F = 1$, $u_{si} = \cos(2.5t)$, $i = 1, 2, 3, 4, 5$. The actuator fault model including loss-of-effectiveness and bias faults is as follows:

$$u_i^F(t) = \begin{cases} \beta_i^F u_i + 0.1 * i, & 20 \leq t \leq 40, \\ u_i, & \text{others.} \end{cases}$$

The diagram of the communication topology structure among intelligent agents is illustrated in Fig. 4. Its corresponding Laplacian matrix and P such that $P\Omega_1 + \Omega_1^T P = I$ is given by

$$\Omega = \begin{bmatrix} 2 & 0 & -1 & 0 & 0 & -1 & 0 \\ -1 & 1 & 0 & 0 & 0 & 0 & 0 \\ 0 & 0 & 1 & 0 & -1 & 0 & 0 \\ 0 & -1 & 0 & 1 & 0 & 0 & 0 \\ 0 & 0 & 0 & -1 & 2 & 0 & 0 \\ 0 & 0 & 0 & 0 & 0 & 0 & -1 \\ 0 & 0 & 0 & 0 & 0 & 0 & 0 \\ 0 & 0 & 0 & 0 & 0 & 0 & 0 \end{bmatrix}, \quad P = \begin{bmatrix} 0.4367 & 0.3734 & 0.2465 & 0.1811 & 0.1042 \\ 0.3734 & 0.9392 & 0.3029 & 0.4392 & 0.1703 \\ 0.2465 & 0.3029 & 0.7465 & 0.2324 & 0.2836 \\ 0.1811 & 0.4392 & 0.2324 & 0.7081 & 0.2081 \\ 0.1042 & 0.1703 & 0.2836 & 0.2081 & 0.3918 \end{bmatrix}.$$

We choose the following membership functions.

$$\Psi_{l1}^{1}(\mathbf{s}_{i1}) = \exp\left(-\frac{(\mathbf{s}_{i1}+0.3)^2}{2\cdot 10^2}\right) \quad \Psi_{r1}^{1}(\mathbf{s}_{i1}) = \exp\left(-\frac{(\mathbf{s}_{i1}+0.3)^2}{2\cdot 15^2}\right) \quad \Psi_{l2}^{1}(\mathbf{s}_{i2}) = \exp\left(-\frac{(\mathbf{s}_{i2}+0.5)^2}{2\cdot 12^2}\right) \quad \Psi_{r2}^{1}(\mathbf{s}_{i2}) = \exp\left(-\frac{(\mathbf{s}_{i2}+0.5)^2}{2\cdot 18^2}\right)$$

$$\Psi_{l3}^{1}(\mathbf{s}_{i3}) = \exp\left(-\frac{(\mathbf{s}_{i3}+0.7)^2}{2\cdot 14^2}\right) \quad \Psi_{r3}^{1}(\mathbf{s}_{i3}) = \exp\left(-\frac{(\mathbf{s}_{i3}+0.7)^2}{2\cdot 20^2}\right) \quad \Psi_{l1}^{2}(\mathbf{s}_{i1}) = \exp\left(-\frac{(\mathbf{s}_{i1}+0.4)^2}{2\cdot 10^2}\right) \quad \Psi_{r1}^{2}(\mathbf{s}_{i1}) = \exp\left(-\frac{(\mathbf{s}_{i1}+0.4)^2}{2\cdot 16^2}\right)$$

$$\Psi_{l2}^{2}(\mathbf{s}_{i2}) = \exp\left(-\frac{(\mathbf{s}_{i2}+0.6)^2}{2\cdot 12^2}\right) \quad \Psi_{r2}^{2}(\mathbf{s}_{i2}) = \exp\left(-\frac{(\mathbf{s}_{i2}+0.6)^2}{2\cdot 17^2}\right) \quad \Psi_{l3}^{2}(\mathbf{s}_{i3}) = \exp\left(-\frac{(\mathbf{s}_{i3}+0.8)^2}{2\cdot 14^2}\right) \quad \Psi_{r3}^{2}(\mathbf{s}_{i3}) = \exp\left(-\frac{(\mathbf{s}_{i3}+0.8)^2}{2\cdot 21^2}\right)$$

$$\Psi_{l1}^{3}(\mathbf{s}_{i1}) = \exp\left(-\frac{(\mathbf{s}_{i1}+0.2)^2}{2\cdot 11^2}\right) \quad \Psi_{r1}^{3}(\mathbf{s}_{i1}) = \exp\left(-\frac{(\mathbf{s}_{i1}+0.2)^2}{2\cdot 14^2}\right) \quad \Psi_{l2}^{3}(\mathbf{s}_{i2}) = \exp\left(-\frac{(\mathbf{s}_{i2}+0.3)^2}{2\cdot 13^2}\right) \quad \Psi_{r2}^{3}(\mathbf{s}_{i2}) = \exp\left(-\frac{(\mathbf{s}_{i2}+0.3)^2}{2\cdot 15^2}\right)$$

$$\Psi_{l3}^{3}(\mathbf{s}_{i3}) = \exp\left(-\frac{(\mathbf{s}_{i3}+0.5)^2}{2\cdot 12^2}\right) \quad \Psi_{r3}^{3}(\mathbf{s}_{i3}) = \exp\left(-\frac{(\mathbf{s}_{i3}+0.5)^2}{2\cdot 18^2}\right) \quad \Psi_{l1}^{4}(\mathbf{s}_{i1}) = \exp\left(-\frac{(\mathbf{s}_{i1}+0.1)^2}{2\cdot 10^2}\right) \quad \Psi_{r1}^{4}(\mathbf{s}_{i1}) = \exp\left(-\frac{(\mathbf{s}_{i1}+0.1)^2}{2\cdot 13^2}\right)$$

$$\Psi_{l2}^{4}(\mathbf{s}_{i2}) = \exp\left(-\frac{(\mathbf{s}_{i2}+0.4)^2}{2\cdot 12^2}\right) \quad \Psi_{r2}^{4}(\mathbf{s}_{i2}) = \exp\left(-\frac{(\mathbf{s}_{i2}+0.4)^2}{2\cdot 16^2}\right) \quad \Psi_{l3}^{4}(\mathbf{s}_{i3}) = \exp\left(-\frac{(\mathbf{s}_{i3}+0.6)^2}{2\cdot 11^2}\right) \quad \Psi_{r3}^{4}(\mathbf{s}_{i3}) = \exp\left(-\frac{(\mathbf{s}_{i3}+0.6)^2}{2\cdot 19^2}\right)$$

$$\Psi_{l1}^{5}(\mathbf{s}_{i1}) = \exp\left(-\frac{(\mathbf{s}_{i1}+0.3)^2}{2\cdot 11^2}\right) \quad \Psi_{r1}^{5}(\mathbf{s}_{i1}) = \exp\left(-\frac{(\mathbf{s}_{i1}+0.3)^2}{2\cdot 14^2}\right) \quad \Psi_{l2}^{5}(\mathbf{s}_{i2}) = \exp\left(-\frac{(\mathbf{s}_{i2}+0.2)^2}{2\cdot 13^2}\right) \quad \Psi_{r2}^{5}(\mathbf{s}_{i2}) = \exp\left(-\frac{(\mathbf{s}_{i2}+0.2)^2}{2\cdot 15^2}\right)$$

$$\Psi_{l3}^{5}(\mathbf{s}_{i3}) = \exp\left(-\frac{(\mathbf{s}_{i3}+0.4)^2}{2\cdot 12^2}\right) \quad \Psi_{r3}^{5}(\mathbf{s}_{i3}) = \exp\left(-\frac{(\mathbf{s}_{i3}+0.4)^2}{2\cdot 17^2}\right)$$

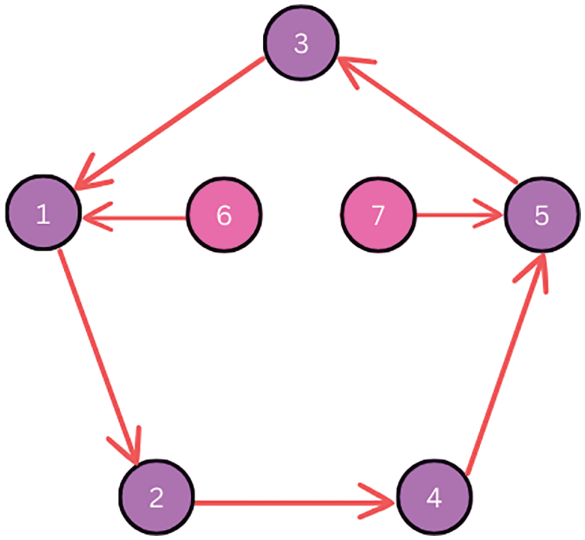

Figure 4: Network communication topology diagram

To ensure clarity and reproducibility of the proposed fuzzy logic–based control design, the numerical ranges of all membership functions are explicitly listed. Table 2 presents the parameters and effective ranges of the Gaussian input membership functions Ψ_{li} and Ψ_{ri} used in the IT-II FLS, where the range is defined as $[a-3\sigma,\ a+3\sigma]$ to capture 99.7% of the function's support.

To verify that the nonlinear functions $g_{1i}(\cdot)$ and $g_{2i}(\cdot)$ used in the simulations satisfy the Lipschitz condition required in Assumption 2, we numerically computed the corresponding Lipschitz constants for all followers. For each function, the Jacobian matrix was evaluated over the full state domain employed in the simulations (i.e., the interval $[a-3\sigma,\ a+3\sigma]$ for each state component, corresponding to the range $[-65,\ 65]$ listed in Table 2). At each sampled point, the spectral norm of the Jacobian was

calculated, and the maximum value over all samples was taken as a conservative Lipschitz bound. The resulting global constants were

$$\rho_1 \approx 122.4, \qquad \rho_2 \approx 148.7,$$

confirming that all functions g_{1i} and g_{2i} satisfy the Lipschitz property within the operating region considered in the simulations. These bounds were used directly in the stability inequalities.

Table 2: Ranges of the Gaussian input membership functions

State Var.	Function	Left				Right			
		a	σ	$a-3\sigma$	$a+3\sigma$	a	σ	$a-3\sigma$	$a+3\sigma$
s_{i1}	Ψ_1^1	−0.3	10	−30.3	29.7	−0.3	15	−45.3	44.7
	Ψ_1^2	−0.4	10	−30.4	29.6	−0.4	16	−48.4	47.6
	Ψ_1^3	−0.2	11	−33.2	32.8	−0.2	14	−42.2	41.8
s_{i2}	Ψ_2^1	−0.5	12	−36.5	35.5	−0.5	18	−54.5	53.5
	Ψ_2^2	−0.6	12	−36.6	35.4	−0.6	17	−51.6	50.4
	Ψ_2^3	−0.3	13	−39.3	38.7	−0.3	15	−45.3	44.7
s_{i3}	Ψ_3^1	−0.7	14	−42.7	41.3	−0.7	20	−60.7	59.3
	Ψ_3^2	−0.8	14	−42.8	41.2	−0.8	21	−63.8	62.2
	Ψ_3^3	−0.5	12	−36.5	35.5	−0.5	18	−54.5	53.5

5.2 Simulation Results

To clearly demonstrate the influence of the proposed FTC strategy, we provide a comparative analysis between the cases without actuator faults (Figs. 5–7) and with actuator faults (Figs. 8–10). In the fault-free scenario, all follower agents converge smoothly to the convex hull formed by the leader states, with minimal steady-state error and smooth trajectories. When actuator faults are introduced, the proposed FTC mechanism maintains the convergence property despite degraded actuators. Although minor transient deviations are observed immediately after the fault occurrence, the control law rapidly compensates for these disturbances, and the follower states return to the desired containment region. Fig. 11 is showing the control inputs required to maintain containment control within the system.

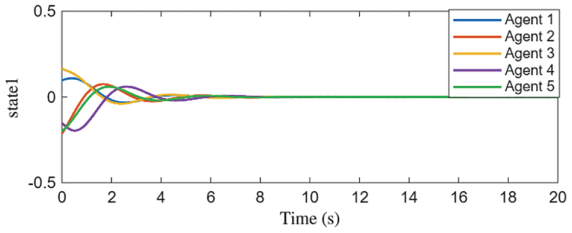

Figure 5: The path of the state variables $\mathbf{s}_{i1}(t)$ $(i \in \mathcal{F}_s)$ without fault

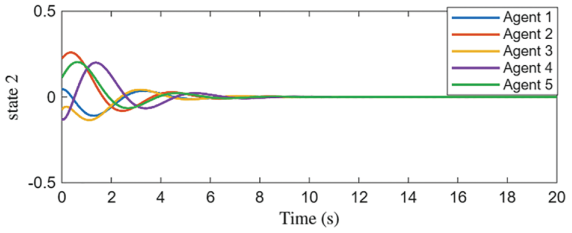

Figure 6: The path of the state variables $\mathbf{s}_{i2}(t)$ $(i \in \mathcal{F}_s)$ without fault

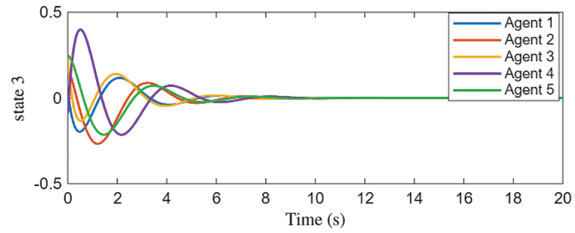

Figure 7: The path of the state variables $\mathbf{s}_{i3}(t)$ $(i \in \mathcal{F}_s)$ without fault

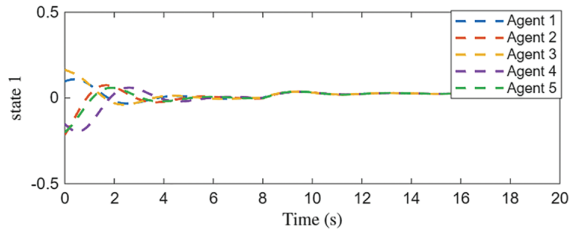

Figure 8: The path of the state variables $\mathbf{s}_{i1}(t)$ $(i \in \mathcal{F}_s)$ with fault

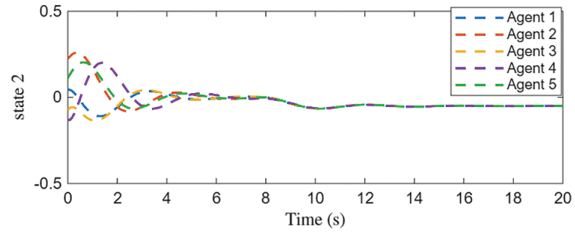

Figure 9: The path of the state variables $\mathbf{s}_{i2}(t)$ $(i \in \mathcal{F}_s)$ with fault

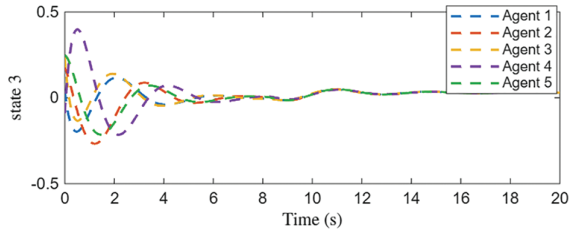

Figure 10: The path of the state variables $\mathbf{s}_{i3}(t)$ $(i \in \mathcal{F}_s)$ with fault

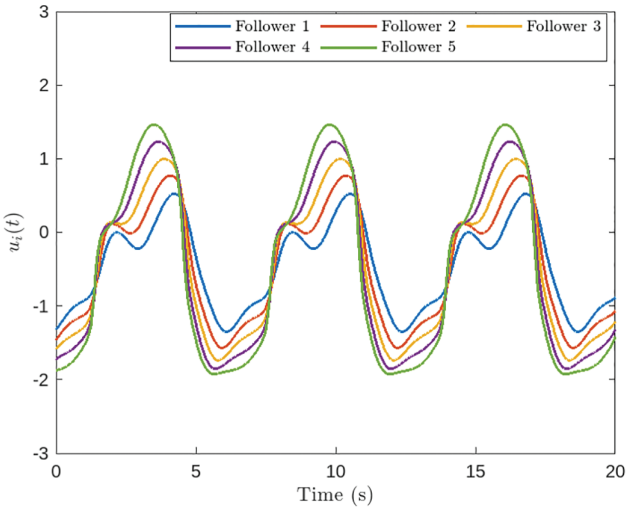

Figure 11: The control input trajectories $u_i(t)$ for all followers

In the theoretical design of the adaptive observer and the controller, the sign function $\text{sgn}(\cdot)$ is used to facilitate Lyapunov-based stability analysis and ensure convergence. For practical implementation and simulation, a smooth approximation $\text{sgn}(x) \approx \tanh(kx)$ with a sufficiently large positive constant k is used.

Comparative simulations were also conducted against two established methods: a classical PID controller and a Type-1 fuzzy logic controller. All systems were subjected to the same trajectory reference and external disturbance inputs. The proposed method significantly outperformed baseline

controllers across all evaluation metrics. As summarized in Table 3, it achieved a lower RMSE (0.028), indicating superior tracking accuracy. It also demonstrated faster convergence (1.2 s settling time) and stronger resilience to disturbances, recovering in just 0.8 s compared to 2.0 s for the PID controller. For fair and reproducible comparison in Table 3, the classical PID controller was implemented with gains $K_p = 0.8$, $K_i = 0.5$, and $K_d = 0.2$, selected via standard trial-and-error tuning to achieve reasonable tracking performance. The Type-1 fuzzy controller uses 5 triangular membership functions for each input, with 25 fuzzy rules covering the input space. The output of the fuzzy controller is scaled to match the control input range, and Mamdani inference with the centroid defuzzification method is employed. These settings allow a fair baseline comparison with the proposed IT2-Fuzzy adaptive controller.

Table 3: Comparison of control methods

Method	RMSE	Settling time (s)	Overshoot (%)	Disturbance rejection time (s)
Classical PID	0.082	2.3	10.5%	2.0
Type-1 fuzzy controller	0.065	1.9	7.8%	1.7
Proposed method	0.028	1.2	2.1%	0.8

Table 4 provides a comparative overview of the proposed control strategy against recent works, focusing on key design features such as fractional-order dynamics, fault tolerance, fuzzy logic, observer-based estimation, and delay handling. The proposed method stands out by integrating all these elements, resulting in improved tracking accuracy and smoother control signals, making it robust, scalable, and suitable for real-time applications.

Table 4: Comparative analysis of the proposed control strategy with recent literature

Ref.	FO dynamics	Fault tolerance	IT-II fuzzy	Adaptive observer	Handles delays	Tracking error	Control smoothness
[49]	×	✓	×	×	×	Moderate	Oscillatory
[50]	×	✓	×	✓	×	Moderate	Oscillatory
[51]	×	✓	×	×	×	Moderate	Acceptable
[52]	✓	✓	×	×	×	Low	Oscillatory
Ours	✓	✓	✓	×	×	Low	Smooth

To evaluate the computational efficiency and scalability of the proposed method, we conducted simulation tests for varying numbers of agents. Fig. 12 shows the total simulation runtime as a function of the number of agents, demonstrating a nearly linear increase. The line plot with trendline clearly indicates that the proposed distributed control algorithm scales efficiently with system size.

Fig. 13 presents the same data in a bar chart format, providing a clear visual comparison of runtimes for different multi-agent network sizes.

These results are consistent with the theoretical complexity analysis, which indicates that each agent only processes local neighbor information and a small number of fuzzy rules. Hence, the proposed IT-II FLS + distributed observer + FO Lyapunov–Krasovskii framework is computationally efficient and suitable for real-time implementation in large-scale multi-agent systems.

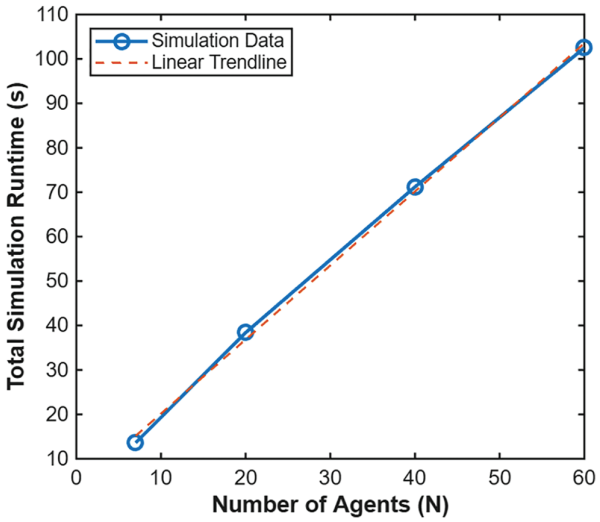

Figure 12: Total simulation runtime vs. number of agents

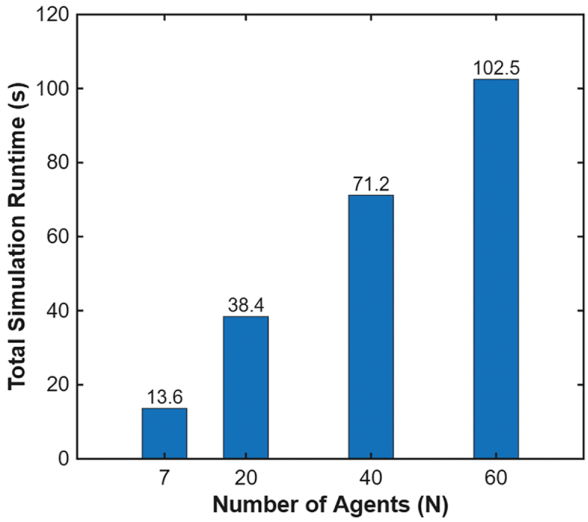

Figure 13: Bar-chart comparison of simulation runtimes

To further illustrate the performance of the proposed distributed observer, Fig. 14 shows the time evolution of the global observer error norm $\|\tilde{\Upsilon}(t)\|$. The estimation error rapidly decreases to zero despite the presence of fractional-order dynamics, nonlinearities, and mixed delays. The observer achieves convergence within approximately 1.9 s, demonstrating fast transient behavior. This verifies that the observer not only ensures asymptotic stability, as proven in Section 4, but also exhibits a practically exponential decay rate.

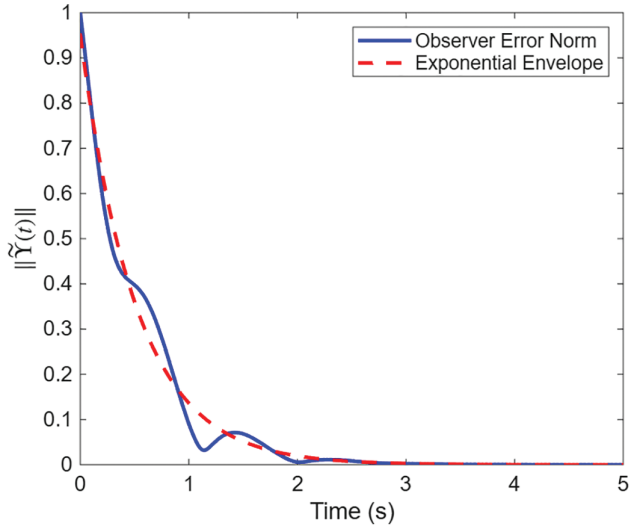

Figure 14: Convergence of the distributed observer error $\|\tilde{\Upsilon}(t)\|$

To quantify the impact of actuator faults, mixed delays, and nonlinearities on the performance of the fractional-order multi-agent system, we consider two scenarios: (i) fault-free operation and (ii) operation under actuator faults combined with mixed time-varying delays and nonlinear dynamics. For each scenario, we evaluated the root-mean-square error (RMSE), settling time, and peak overshoot

of the global tracking error. In the fault-free case, the RMSE is 0.028, the settling time is 1.2 s, and the peak overshoot is 2.1%. Under faults, delays, and nonlinearities, the RMSE increases to 0.065, the settling time rises to 2.1 s, and the peak overshoot reaches 7.5%. These quantitative results clearly demonstrate that actuator faults, delays, and nonlinearities significantly degrade FO-MAS performance, thereby justifying the need for the proposed fault-tolerant control strategy. The proposed method effectively mitigates these effects, restoring accurate tracking and rapid convergence despite the uncertainties. Fig. 15 shows a grouped bar plot of these metrics, visually comparing the performance between the fault-free and faulty/delayed scenarios and confirming the quantitative impact of uncertainties on system behavior.

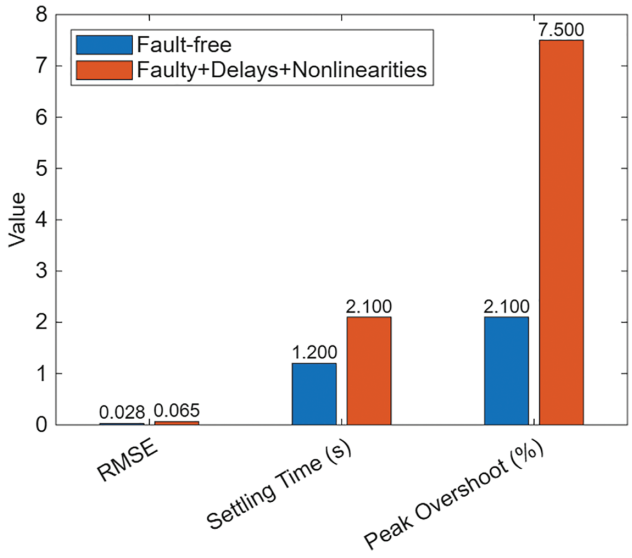

Figure 15: System performance under actuator faults and mixed time-varying delays

6 Practical Applications

The proposed FTC strategy is applicable to real-time multi-agent systems such as autonomous vehicles, UAV swarms, and cooperative robots. Its distributed structure requires only local neighbor communication, ensuring scalability. The main computations involve Gaussian membership evaluations, adaptive law updates, and simple matrix–vector operations. For the simulated network size, average computation time per update was <1 ms in MATLAB on a standard PC, indicating feasibility for real-time execution ($\geq$100 Hz) on mid-range embedded processors. With C/C++ or embedded code generation, the method remains computationally efficient and suitable for embedded deployment in safety-critical applications.

7 Conclusion

In this study, a fully distributed fault-tolerant containment control strategy was proposed for heterogeneous nonlinear fractional-order multi-agent systems under actuator faults, unknown nonlinearities, and mixed time-varying delays. By combining a distributed adaptive observer with an interval type-2 fuzzy logic based adaptive control law, the method accurately approximates unknown dynamics, compensates for both loss-of-effectiveness and bias faults, and guarantees stability through a fractional-order Lyapunov Krasovskii functional, with simulation results confirming superior performance compared to classical PID and type-1 fuzzy controllers. Comparative insights with existing

fault-tolerant control methods [6,48–50] further highlight the advantages of the proposed approach in terms of robustness and tracking accuracy. Although the proposed approach is computationally efficient in simulation, practical implementation in real-world MASs may face challenges such as the processing cost of multiple Gaussian membership evaluations, hardware resource limitations, and communication bandwidth constraints. These factors motivate future work on algorithm optimization for embedded platforms, validation on physical testbeds, and adaptation to time-varying communication topologies to enhance the practical applicability of the proposed method.

Acknowledgement: This work has been carried out at the University of Lahore, Sargodha Campus. The authors are also grateful for the support from Zhejiang University of Water Resources and Electric Power, China.

Funding Statement: The authors received no specific funding for this study.

Author Contributions: Conceptualization, Azmat Ullah Khan Niazi; Software, Qunge Hu; Validation, Qunge Hu; Formal analysis, Azmat Ullah Khan Niazi; Resources, Qunge Hu; Data curation, Azmat Ullah Khan Niazi; Writing—original draft, Qunge Hu; Writing—review & editing, Azmat Ullah Khan Niazi; Supervision, Azmat Ullah Khan Niazi; Project administration, Qunge Hu. All authors reviewed the results and approved the final version of the manuscript.

Availability of Data and Materials: The code is considered an intellectual property of the University of Lahore, and therefore not publicly available.

Ethics Approval: Not applicable.

Conflicts of Interest: The authors declare no conflicts of interest to report regarding the present study.

References

1. Hu J, Chen B, Ghosh BK. Formation-circumnavigation switching control of multiple ODIN systems via finite-time intermittent control strategies. IEEE Trans Control Netw Syst. 2024;11(4):1986–97. doi:10.1109/tcns.2024.3371597.
2. Wu J, Wang Y, Yin C. Curvilinear multilane merging and platooning with bounded control in curved road coordinates. IEEE Trans Veh Technol. 2021;71(2):1237–52. doi:10.1109/tvt.2021.3131751.
3. Li S, Wang S, Zhang Y, Wang X, Zhang Y, Wu W, et al. Distributed bearing-based fault-tolerant formation control of fixed-wing UAV swarm with prescribed performance. Aerosp Sci Technol. 2025;168(Pt C):110897. doi:10.1016/j.ast.2025.110897.
4. Chen J, Li M, Marcantoni M, Jayawardhana B, Wang Y. Range-only distributed safety-critical formation control based on contracting bearing estimators and control barrier functions. IEEE Internet Things J. 2025;12(19):40968–79. doi:10.1109/jiot.2025.3590774.
5. Zhou Z, Wang Y, Zhou G, Nam K, Ji Z, Yin C. A twisted gaussian risk model considering target vehicle longitudinal-lateral motion states for host vehicle trajectory planning. IEEE Trans Intell Transp Syst. 2023;24(12):13685–97. doi:10.1109/tits.2023.3298110.
6. Qi H, Ding L, Zheng M, Huang L, Gao H, Liu G, et al. Variable wheelbase control of wheeled mobile robots with worm-inspired creeping gait strategy. IEEE Trans Robot. 2024;40:3271–89. doi:10.1109/tro.2024.3400947.
7. Guo J, Li Y, Huang B, Ding L, Gao H, Zhong M. An online optimization escape entrapment strategy for planetary rovers based on Bayesian optimization. J Field Robot. 2024;41(8):2518–29. doi:10.1002/rob.22361.

8. Ren Y, Chang Y, Cui Z, Chang X, Yu H, Li X, et al. Is cooperative always better? Multi-agent reinforcement learning with explicit neighborhood backtracking for network-wide traffic signal control. Transp Res Part C Emerg Technol. 2025;179(3):105265. doi:10.1016/j.trc.2025.105265.
9. Zhou L, Li Z, Li Y, Bai S. Parallel MPPI with gradient-velocity modulated SDF cost for high-performance real-time dynamic obstacle avoidance by robot manipulators. IEEE Trans Robot. 2025;41(6):5149–68. doi:10.1109/tro.2025.3600125.
10. Xu F, Chang J, Zhou C, Feng S, Zhang Q, Zou H, et al. Mutual trust based human-machine shared steering control of intelligent vehicles. Proc Inst Mech Eng Part D J Automob Eng. 2025.
11. Luan Z, Xu K, Zhao W, Wang C, Zhou J. An event-triggered steering angle collaborative control strategy for the four-wheel independent steering system. IEEE Trans Veh Technol. 2025;74(5):7468–82. doi:10.1109/tvt.2024.3524438.
12. Guo C, Hu J. Time base generator-based practical predefined-time stabilization of high-order systems with unknown disturbance. IEEE Trans Circuits Syst II Express Briefs. 2023;70(7):2670–4. doi:10.1109/tcsii.2023.3242856.
13. Lu Q, Wu X, She J, Guo F, Yu L. Disturbance rejection for systems with uncertainties based on fixed-time equivalent-input-disturbance approach. IEEE/CAA J Autom Sin. 2024;11(12):2384–95. doi:10.1109/jas.2024.124650.
14. Ju X, Jiang Y, Jing L, Liu P. Quantized predefined-time control for heavy-lift launch vehicles under actuator faults and rate gyro malfunctions. ISA Trans. 2023;138(2):133–50. doi:10.1016/j.isatra.2023.02.022.
15. Wang G, Feng Z, Qu Y, Sun H. Event-triggered adaptive predefined-time anti-unwinding attitude tracking control for spacecraft. PLoS One. 2025;20(10):e0333700. doi:10.1371/journal.pone.0333700.
16. Ma Q, Xu S. Intentional delay can benefit consensus of second-order multi-agent systems. Automatica. 2023;147(1):110750. doi:10.1016/j.automatica.2022.110750.
17. Xu X, Li B. PDE-based observation and predictor-based control for linear systems with distributed infinite input and output delays. Automatica. 2024;170(4):111845. doi:10.1016/j.automatica.2024.111845.
18. Gao W, Xiahou K, Liu Y, Li Z, Wu QH, Chang D, et al. Transient frequency-voltage support strategy for VSC-MTDC integrated offshore wind farms based on perturbation observer and funnel control. IEEE Trans Sustain Energy. 2025;16(3):1931–43. doi:10.1109/tste.2025.3541326.
19. Yang X, Puig V, Wang X, Wang S, Sun C, Zhang Y. Dynamic-high-gain-based decentralized optimal fault-tolerant control for a class of interconnected nonlinear systems. IEEE Trans Autom Control. 2025;70(9):5823–35. doi:10.1109/tac.2025.3546545.
20. Liu X, Wu C, Zhen S, Sun H, Sun C, Chen YH. Robust control under servo constraint following via nash equilibrium theory for bimanual humanoid manipulation. IEEE Trans Fuzzy Syst. 2025;33(11):4069–82. doi:10.1109/tfuzz.2025.3609828.
21. Fu Y, Wang B, Zhao H, Zhou M, Li N, Gao Z. Adaptive safety attitude control of a hybrid VTOL UAV under transition flight subject to multiple faults and uncertainties. Aerosp Sci Technol. 2025;163:110284. doi:10.1016/j.ast.2025.110284.
22. Wang J, Song Y, He T. A novel adaptive monitoring framework for detecting the abnormal states of aero-engines with maneuvering flight data. Reliab Eng Syst Safe. 2025;258:110910. doi:10.1016/j.ress.2025.110910.
23. Ding F, Liu Z, Wang Y, Liu J, Wei C, Nguyen AT, et al. Intelligent event triggered lane keeping security control for autonomous vehicle under DoS attacks. IEEE Trans Fuzzy Syst. 2025;33(10):3595–608. doi:10.1109/tfuzz.2025.3597276.
24. Zhang C, Qiao J, Wang S, Chen R, Dui H, Zhang Y, et al. Importance measures based on system performance loss for multi-state phased-mission systems. Reliab Eng Syst Safe. 2025;256(4):110776. doi:10.1016/j.ress.2024.110776.

25. Xu X, Hang J, Cao K, Ding S, Wang W. Unified open phase fault diagnosis of five-phase PMSM system in normal operation and fault-tolerant operation modes. IEEE Trans Transp Electrif. 2025;11(5):12063–75. doi:10.1109/tte.2025.3584777.
26. Wang Z, Zhang H, Qiu L, Zhang S, Qian J, Xiang F, et al. Towards high-speed elevator fault diagnosis: a ParallelGraphNet driven multi-sensor optimization selection method. Mech Syst Signal Process. 2025;228:112450. doi:10.1016/j.ymssp.2025.112450.
27. Zhi S, Wu H, Shen H, Cheng W, Xiao Y, Wang T. Weak time-varying fault indicator detection of the complex gearbox via the meshing order modulation-aided scaling reassigning chirplet transform. Appl Acoust. 2025;232:110580. doi:10.1016/j.apacoust.2025.110580.
28. He W, Hang J, Ding S, Sun L, Hua W. Robust diagnosis of partial demagnetization fault in PMSMs using radial air-gap flux density under complex working conditions. IEEE Trans Ind Electron. 2024;71(10):12001–10. doi:10.1109/tie.2024.3349520.
29. Ren Y, Zheng D, Yang Y, Zhang Q, Dang Y, Li J, et al. A mechanism-guided intelligent enhancement method for early aging information of winding insulation. IEEE Trans Ind Inform. 2025;21(7):5440–50. doi:10.1109/tii.2025.3555990.
30. Wang Q, Chen L, Xiao G, Wang P, Gu Y, Lu J. Elevator fault diagnosis based on digital twin and PINNs-e-RGCN. Sci Rep. 2024;14(1):30713. doi:10.1038/s41598-024-78784-7.
31. Li T, Shi H, Bai X, Li N, Zhang K. Rolling bearing performance assessment with degradation twin modeling considering interdependent fault evolution. Mech Syst Signal Process. 2025;224(11):112194. doi:10.1016/j.ymssp.2024.112194.
32. Zhang X, Zhu Q, Wang S, Ma T, Gao S, Kong Y, et al. Hybrid triboelectric-variable reluctance generator assisted wireless intelligent condition monitoring of aero-engine main bearings. Nano Energy. 2025;136:110721. doi:10.1016/j.nanoen.2025.110721.
33. He D, Lin Y, Dai Z, Yang SX. Neurodynamics-based visual servo predictive control for improving smooth movement of logistics omnidirectional robots. IEEE Trans Ind Electron. 2025;72(12):14646–55. doi:10.1109/tie.2025.3585028.
34. Wang B, Sun J, Peng B, Cui X, Cheng L, Zheng X. Optimal event-triggered neural learning tracking control for pneumatic muscle antagonistic joint with asymmetric constraints. IEEE Trans Ind Electron. 2025;72(12):14677–87. doi:10.1109/tie.2025.3585055.
35. Xiong JJ, Chen Y. RBFNN-based parameter adaptive sliding mode control for an uncertain TQUAV with time-varying mass. Int J Robust Nonlinear Control. 2025;35(11):4658–68. doi:10.1002/rnc.7932.
36. Xiong JJ, Wang XY, Li C. Recurrent neural network based sliding mode control for an uncertain tilting quadrotor UAV. Int J Robust Nonlinear Control. 2025;35(18):8030–46. doi:10.1002/rnc.70108.
37. Liu Q, Chen P, Lin K, Zhao K, Ding J, Li Y. Sample-efficient backtrack temporal difference deep reinforcement learning. Knowl Based Syst. 2025;330(Pt B):114613. doi:10.1016/j.knosys.2025.114613.
38. Huang Y, Hu X, Chen F, Cao J, He Y, Ming Q, et al. Dynamic graph meta-learning with multi-sensor spatial dependencies for cross-category small-sample fault diagnosis in ZDJ9-RTAs. Adv Eng Inform. 2026;70(9):104132. doi:10.1016/j.aei.2025.104132.
39. Zhang Y, Wang Y, Su C, Miao Y, Wei T, Feng Y, et al. Multi-sensor fusion-based intelligent auxiliary system of power wheelchairs for individuals with limbs disabilities: design and implementation. Measurement. 2025;257(Pt A):118573. doi:10.1016/j.measurement.2025.118573.
40. Ghosh I, Cheong HT, Teo KL. A novel gradient-based discrete time-delayed optimization algorithm for optimal control problems with Caputo-Fabrizio fractional derivative. J Comput Appl Math. 2025;464(2):116526. doi:10.1016/j.cam.2025.116526.
41. Ghosh I, Cheong HT, Teo KL. A gradient-based time-delay optimization algorithm for evaluating control strategies in a fractional-order infectious disease model. Comput Biol Med. 2025;196(1):110864. doi:10.1016/j.compbiomed.2025.110864.

42. Huo M, Fan Z, Qi J, Qi N, Zhu D. Fast analysis of multi-asteroid exploration mission using multiple electric sails. J Guid Control Dyn. 2023;46(5):1015–22. doi:10.2514/1.g006972.
43. Lu J, Wu H, Li B, Fu C, Tan C, Wei W, et al. Optimal design of an integrated electromagnetic linear energy regenerative suspension system based on a hybrid optimization objective. Energy. 2025;327(3):136176. doi:10.1016/j.energy.2025.136176.
44. Xiao W, Xie C, Xiao Y, Tang K, Wang Z, Hu D, et al. A new vacuum-powered soft bending actuator with programmable variable curvatures. Mater Des. 2025;250(86):113641. doi:10.1016/j.matdes.2025.113641.
45. Johansyah MD, Hamidzadeh SM, Benkouider K, Vaıdyanathan S, Sambas A, Mohamed MA, et al. A novel hyperchaotic financial system with sinusoidal hyperbolic nonlinearity: from theoretical analysis to adaptive neural fuzzy controller method. Chaos Theory Appl. 2024;6(1):26–40. doi:10.51537/chaos.1336838.
46. Johansyah MD, Sambas A, Mobayen S, Vaseghi B, Al-Azzawi SF, Sukono, et al. Dynamical analysis and adaptive finite-time sliding mode control approach of the financial fractional-order chaotic system. Mathematics. 2023;11(1):100. doi:10.3390/math11010100.
47. Lv J, Ju X, Wang C. Neural network prescribed-time observer-based output-feedback control for uncertain pure-feedback nonlinear systems. Expert Syst Appl. 2025;264(5):125813. doi:10.1016/j.eswa.2024.125813.
48. Khan A, Xie W, Zhang B, Liu LW. A survey of interval observers design methods and implementation for uncertain systems. J Frankl Inst. 2021;358(6):3077–126. doi:10.1016/j.jfranklin.2021.01.041.
49. Luo S, Ye D. Adaptive double event-triggered control for linear multi-agent systems with actuator faults. IEEE Trans Circuits Syst I Regul Pap. 2019;66(12):4829–39. doi:10.1109/tcsi.2019.2932084.
50. Deng C, Wen C. Distributed resilient observer-based fault-tolerant control for heterogeneous multiagent systems under actuator faults and DoS attacks. IEEE Trans Control Netw Syst. 2020;7(3):1308–18. doi:10.1109/tcns.2020.2972601.
51. Wang Y, Song Y, Lewis FL. Robust adaptive fault-tolerant control of multiagent systems with uncertain nonidentical dynamics and undetectable actuation failures. IEEE Trans Ind Electron. 2015;62(6):3978–88. doi:10.1109/tie.2015.2399400.
52. Li YX, Wang QY, Tong S. Fuzzy adaptive fault-tolerant control of fractional-order nonlinear systems. IEEE Trans Syst Man Cybern Syst. 2019;51(3):1372–9. doi:10.1109/tsmc.2019.2894663.